

The official publication of the
Hong Kong Academy of Medicine and
the Hong Kong Medical Association

HONG KONG

MEDICAL JOURNAL

香港醫學雜誌

25(S5)

HONG KONG MEDICAL JOURNAL

香港醫學雜誌

Volume 25 Number 4 August 2019

Health and Medical Research Fund

Research Dissemination Reports

醫療衛生研究基金

研究成果報告

Stroke
中風

Neurology
神經內科

Congenital Disorders
先天性疾病

Vision Science
視覺科學

ISSN 1024-2708



香港醫學專科學院出版社
HONG KONG ACADEMY OF MEDICINE PRESS

Supplement 5

MEDICAL JOURNAL

香港醫學雜誌

EDITOR-IN-CHIEF

Martin CS Wong 黃至生

SENIOR EDITORS

LW Chu 朱亮榮
 Albert KK Chui 徐家強
 Michael G Irwin
 Eric CH Lai 賴俊雄
 KY Leung 梁國賢
 Anthony CF Ng 吳志輝
 TW Wong 黃大偉

EDITORS

KS Chan 陳健生
 Jacqueline PW Chung 鍾佩樺
 James TK Fung 馮德焜
 Brian SH Ho 何思灝
 Ellis KL Hon 韓錦倫
 KW Huang 黃凱文
 WK Hung 熊維嘉
 Bonnie CH Kwan 關清霞
 Arthur CW Lau 劉俊穎
 PY Lau 婁培友
 Danny WH Lee 李偉雄
 Thomas WH Leung 梁慧康
 WK Leung 梁惠強
 Kenneth KW Li 李啟煌
 Janice YC Lo 羅懿之
 Herbert HF Loong 龍浩鋒
 James KH Luk 陸嘉熙
 Arthur DP Mak 麥敦平
 Henry KF Mak 麥嘉豐
 Martin W Pak 白威
 Walter WK Seto 司徒偉基
 Regina WS Sit 薛詠珊
 William YM Tang 鄧旭明
 Jeremy YC Teoh 張源津
 KY Tse 謝嘉瑜
 Harry HX Wang 王皓翔
 HL Wong 黃學良
 Kenneth KY Wong 黃格元
 Patrick CY Woo 胡劍逸
 Hao Xue 薛浩
 Bryan PY Yan 甄秉言
 TK Yau 游子覺
 Kelvin KH Yiu 姚啟恒

EPIDEMIOLOGY ADVISERS

Daniel SY Ho 何世賢
 Edmond SK Ma 馬紹強
 Gary Tse 謝家偉
 Shelly LA Tse 謝立亞
 Ian YH Wong 王逸軒
 Esther YT Yu 余懿德
 Hunter KL Yuen 袁國禮

STATISTICAL ADVISERS

Marc KC Chong 莊家俊
 William B Goggins
 Eddy KF Lam 林國輝
 Carlos KH Wong 黃競浩

HONORARY ADVISERS

David VK Chao 周偉強
 Paul BS Lai 賴寶山

Health and Medical Research Fund**Research Dissemination Reports****Health Research Symposium 2019: Genomics and Big Data in Health and Disease** 3*RA Collins, ESK Ma***STROKE****Risk of intracerebral haemorrhage in patients with cerebral microbleeds taking warfarin for atrial fibrillation: a prospective study** 6*YO Soo, J Abrigo, W Chu, KT Leung, WC Fong, SH Li, R Li, PW Ng, KK Wong, LKS Wong, TWH Leung***Autonomic dysfunction as measured by Ewing battery test to predict poor outcome after acute ischaemic stroke** 9*L Xiong, G Tian, HW Leung, XY Chen, WH Lin, TWH Leung, YO Soo, DYW Siu, LKS Wong***Dedifferentiation-reprogrammed mesenchymal stem cells for neonates with hypoxic-ischaemic brain injury** 12*FY Yang, XH Zhang, LL Tsang, HC Chan, XH Jiang***Topically applied adipose-derived mesenchymal stem cell treatment in experimental focal cerebral ischaemia** 17*GKC Wong, PK Lam, AWI Lo, AKY Chan, YX Wang, WS Poon***Effects of collateral circulation on haemodynamic flow status in intracranial artery stenosis depicted by computational fluid dynamics** 18*TWH Leung, SY Fan, HL Ip, AYL Lau, DYW Siu, EYL Dai, LKS Wong, DS Liebeskind***NEUROLOGY****Neutralising antibodies to interferon-beta therapy in relapsing multiple sclerosis: a pilot study** 22*AYL Lau, E Chan, KK Lau, V Mok, DYW Siu, R Lee***Novel beta-amyloid aggregate inhibitors for Alzheimer's disease** 26*RMS Wong, HW Li, DWJ Kwong, KKL Yung, Y Ke*

**INTERNATIONAL EDITORIAL
ADVISORY BOARD**

Sabarathnam Arulkumaran
United Kingdom

Robert Atkins
Australia

Peter Cameron
Australia

Daniel KY Chan
Australia

David Christiani
United States

Andrew Coats
Australia

James Dickinson
Canada

Willard Fee, Jr
United States

Robert Hoffman
United States

Sean Hughes
United Kingdom

Roger Jones
United Kingdom

Michael Kidd
Australia

Arthur Kleinman
United States

Stephen Leeder
Australia

Xiaoping Luo
PR China

William Rawlinson
Australia

Jonathan Samet
United States

Yaojiang Shi
PR China

David Weller
United Kingdom

Max Wintermark
United States

Atsuyuki Yamataka
Japan

Homer Yang
Canada

KG Yeoh
Singapore

Matthew Yung
United Kingdom

Zhijie Zheng
PR China

Full details of the Editorial Board
are available online at
<https://www.hkmj.org/about/eo.html>

MANAGING EDITOR

Alan Purvis

DEPUTY MANAGING EDITOR

Betty Lau 劉薇薇

ASSISTANT MANAGING EDITOR

Warren Chan 陳俊華

CONGENITAL DISORDERS

Prenatal diagnosis of pathogenic genomic imbalance in fetuses with increased nuchal translucency but normal karyotyping using chromosomal microarray 30

TY Leung, KC Au Yeung, WC Leung, KY Leung, TK Lo, WWK To, WL Lau, LW Chan, DS Sahota, RKW Choy

Placental biology of Down syndrome in relation to increased gene dosage 33

OGW Wong, HYS Ngan, ANY Cheung

Whole exome sequencing to uncover genetic variants underlying congenital cystic adenomatoid malformations 36

PK Tam

VISION SCIENCE

Exome sequencing to reveal presymptomatic genetic markers for primary open angle glaucoma 39

LJ Chen, CP Pang, CCY Tham, CKS Leung

Modulation of the PTEN/mTOR pathway to enhance survival of cone photoreceptors in retinal degeneration disorders 44

B Lin

Author index & Disclaimer 48

Health Research Symposium 2019: Genomics and Big Data in Health and Disease

RA Collins, ESK Ma

Research Fund Secretariat, Research Office, Food and Health Bureau, Hong Kong Special Administrative Region Government,
People's Republic of China

The Health Research Symposium 2019, organised by the Food and Health Bureau, was held on 12 June 2019 at the Hong Kong Academy of Medicine Jockey Club Building. The event provided a platform to facilitate dialogues among local researchers on their latest achievements in health-related research and to learn from international experiences. The event aimed to set a benchmark for excellent research in health and medicine and to foster collaboration in research to improve the health of the population. The Symposium was attended by some 500 delegates, including 119 poster presenters.

Prof Sophia Chan Siu-chee, the Secretary for Food and Health, opened the Symposium by welcoming the keynote speakers, distinguished guests, and other participants. Reflecting on the Symposium's theme, Prof Chan noted that genomics and use of health big data were inter-related and covered nearly every aspect of medical and health research including communicable and non-communicable diseases. Research on genomics and big data fully supports the Government's stated priorities in advancing health and medical research in the coming years. Following the Chief Executive's 2017 Policy Address, the Steering Committee on Genomic Medicine was set up to consider strategies for developing genomic medicine for better public health policies and clinical outcomes. The Government has allocated about \$1.2 billion to implement the Hong Kong Genome Project, under which 40 000 to 50 000 whole genome sequences will be obtained in the coming 6 years to establish a genome database of the local population, as well as a talent pool and relevant infrastructure. In addition, the Hospital Authority has established a Big Data Analytics Platform to facilitate healthcare-related research and innovation. The pilot stage of the Platform was launched in December 2018; six research projects from different local universities are ongoing. Prof Chan said that the Hospital Authority expected to formally launch the Platform by the end of 2019. All these showcase the Government's strong commitment to promoting clinical application and innovative research on genomic medicine for the benefit of patients and their families.

Keynote Session 1 (Moderator: Prof Yip Shea-ping)

Towards precision medicine

Prof Euan Ashley

*Professor of Medicine, Genetics & Data Science,
Stanford University, USA*

Prof Ashley introduced the concept of precision medicine and highlighted some contributions made by clinical genomics to its origin and evolution. He recapped the rapid advancements in genomic technology and illustrated the utility of genomics for clinical medicine using specific patient examples. Some of the essential algorithmic approaches to the interpretation of human genomes were discussed. Areas where current short read sequencing technologies perform well were identified, as well as areas where new approaches were required. In the context of precision and accuracy in genomics, newer technologies such as long read sequencing and new algorithms for improving test performance in complex areas of the genome were introduced. He also presented the use of gold standards in genomics and the limitations of the human reference genome. Finally, Prof Ashley highlighted the near-term future of clinical genomics. Throughout the talk, illustrative patient examples were used including those from the Undiagnosed Diseases Network.

Genomic study on molecular pathways of cancer development and its relevance to cancer precision medicine

Prof Leung Suet-yi

Associate Dean (Research), YW Kan Professor in Natural Sciences, Chair of Gastrointestinal Cancer Genetics and Genomics, Hereditary Gastrointestinal Cancer Genetic Diagnosis Laboratory, Department of Pathology, Li Ka Shing Faculty of Medicine, The University of Hong Kong

Genomic studies have revealed the molecular diversity and organ-specific differences in pathways of cancer development with therapeutic implications. Using gastrointestinal cancers as a model, gastric and colorectal cancers have been found to share some common oncogenic pathways, yet with marked divergent differential incidence of oncogenic pathway alterations. Some of these molecular alterations are emerging as biomarkers for prognostication, guiding patient treatment and prediction of genetic predisposition for focused preventive screening. Prof Leung explained that emerging technologies including next-generation sequencing could facilitate the discovery of novel

genes or pathways that contribute to development of inherited or sporadic gastrointestinal cancers. Coupled with development of new-generation organoid cancer models, next-generation sequencing enables direct culture of patient cancer cells for drug sensitivity testing, and correlation with genomic changes to identify genomic determinants of drug response. Prof Leung said that overall, coupling genomics and organoid-based drug screening, linking back to patient pathology and therapeutic response can empower the development of precision cancer therapy.

Keynote Session 2 (Moderator: Prof Leung Suet-yi)

Observational data for biomedical discovery

Dr Nicholas Tatonetti

Herbert Irving Assistant Professor of Biomedical Informatics, Departments of Biomedical Informatics, Systems Biology, and Medicine, Columbia University, USA

Dr Tatonetti stated that observation was the starting point of discovery. Based on observations, scientists form hypotheses that are tested and evaluated. In the information age, trillions of observations are made and recorded every day: from online social interactions to emergency room visits. In this new age, Dr Tatonetti observed that researchers must turn to computational algorithms to ‘mine’ for new hypotheses and relationships. Data mining is an emerging field dedicated to training algorithms to recognise patterns in enormous sets of data to automatically identify new hypotheses. Dr Tatonetti discussed how data-mining algorithms could be used to identify unexpected effects of drugs used alone or in combination with other drugs. Drug-drug interactions are an important and understudied public health concern. Drug-drug interactions are difficult and expensive to study because of the complex combinatorial nature of their investigation. Dr Tatonetti described how he developed new methods for mining clinical data and then discovered and validated two previously unknown novel drug-drug interactions, namely paroxetine (selective serotonin reuptake inhibitor) and pravastatin (HMG-CoA reductase inhibitor), which together cause hyperglycaemia, and ceftriaxone (cephalosporin antibiotic) and lansoprazole (proton-pump inhibitor), which together are associated with prolonged QT syndrome. The putative associations have been validated prospectively using animal models.

Data analytics & applications in Hong Kong Hospital Authority: past, present & future

¹ Ms Eva Tsui, ² Dr Anderson Tsang Chun-on

¹ *Chief Manager, Statistics & Workforce Planning Department, Hospital Authority, Hong Kong SAR*

² *Clinical Assistant Professor, Division of Neurosurgery, The University of Hong Kong*

The Hong Kong Hospital Authority has implemented public healthcare IT systems to collect patient-based administrative and clinical data across many areas of healthcare services. Ms Tsui and Dr Tsang illustrated how data analytics and statistical modelling skills have been applied to transform this huge volume of real-world data into useful information and then into actionable insights, to inform clinical service planning and developments, and to improve the healthcare system and population’s health. In one example, Ms Tsui described how a risk-prediction tool was developed to estimate the likelihood of unplanned readmission among individual elderly patients through a logistics regression model over one million episodes. This model relies on 14 predictor variables that have standardised definitions across all public hospitals and sustainable data quality over time. In another example, Dr Tsang described a research study that aimed to develop a rapid automated tool to predict the likelihood of large vessel occlusion based on retrospective data of computed tomographic images and clinical information. After a collaborative input towards the study design, an algorithm using the deep learning convolutional neural network model was developed by researchers at The University of Hong Kong, with predictive performance comparable to other validated instruments.

Sharing session on Research Fellowship Scheme

Two researchers supported by the Research Fellowship Scheme shared what they learned from their training programmes and how they applied the skills acquired in their research projects. Dr Ryan Au Yeung Shiu-lun (School of Public Health, Li Ka Shing Faculty of Medicine, The University of Hong Kong) presented his work on *The causal role of adiponectin and triglycerides in ischemic heart disease using a separate sample Mendelian randomisation analysis from publicly available data*, and Dr Wen Chunyi (Department of Biomedical Engineering, The Hong Kong Polytechnic University) discussed *Photoacoustic molecular imaging of osteoarthritic pain: a proof-of-concept study*.

Award ceremony

The Symposium ended with an award ceremony to acknowledge outstanding researches that have influenced health policy and practice in Hong Kong. The award recipients were as follows:

Excellent Research Awards

Principal applicant	Title
Prof CHIEN Wai-tong The Nethersole School of Nursing, The Chinese University of Hong Kong (Administering institution: The Hong Kong Polytechnic University)	An evaluation of the effectiveness of adherence therapy for patients with schizophrenia: a randomized controlled trial
Dr Richard CHOY Kwong-wai Department of Obstetrics and Gynaecology, The Chinese University of Hong Kong	Clinical application of an established target-enrichment massively parallel sequencing method for genetic screening and diagnosis of hereditary hearing loss patients with normal arrayCGH result
Prof JIN Dong-yan Department of Biochemistry, The University of Hong Kong	Roles of Epstein-Barr virus-encoded miR-BART microRNAs in viral persistence and transformation of epithelial cells
Prof Stephen TSUI Kwok-wing School of Biomedical Sciences, The Chinese University of Hong Kong	Whole exome sequencing to dissect the genetic factors behind developmental delay and learning difficulties
Prof Eliza WONG Lai-yi Jockey Club School of Public Health and Primary Care, The Chinese University of Hong Kong	Validation and valuation of the preference-based health index using EQ-5D-5L in the Hong Kong population
Prof Vincent WONG Wai-sun Department of Medicine and Therapeutics, The Chinese University of Hong Kong	Dietary determinants of endotoxemia and nonalcoholic fatty liver disease: a population study

Excellent Health Promotion Project Award

Principal applicant	Title
Dr Derek CHEUNG Yee-tak School of Public Health, The University of Hong Kong	Promotion and brief intervention of smoking cessation at the smoking hotspots
Dr TANG Hoi-yin Psychogeriatric Team, Division I, Kwai Chung Hospital	A training workshop for foreign domestic workers caring for elderly with dementia at home

The Most Promising Young Researcher Award

Principal applicant	Title
Dr Jasper CHAN Fuk-woo Department of Microbiology, The University of Hong Kong	Epidemiology, seroprevalence, and clinical manifestations of immunodeficiency due to autoantibody against interferon gamma in Hong Kong
Dr Alexander LAU Yuk-lun Department of Medicine and Therapeutics, The Chinese University of Hong Kong	Neutralizing antibodies to interferon-beta therapy in Chinese patients with relapsing and remitting multiple sclerosis: a pilot study

Best Poster Awards

Principal applicant	Title
Dr Larry CHOW Applied Biology and Chemical Technology, The Hong Kong Polytechnic University	The use of a novel synthetic flavonoid to improve bioavailability of paclitaxel: a pharmacokinetic, mechanistic and in vivo efficacy study
Prof Benjamin John COWLING School of Public Health, The University of Hong Kong	Intra-season waning of influenza vaccination effectiveness in children
Dr Esther LAU Yuet-ying Department of Psychology, The Education University of Hong Kong	Effects of sleep disturbances on disrupted affective cognition in individuals with depression
Dr Peggy OR Pui-lai Department of Health and Physical Education, The Education University of Hong Kong	School children: An active role in disease prevention

Dr Chui Tak-yi, JP, Under Secretary for Food and Health, thanked the keynote speakers, moderators, judges, speakers in the parallel sessions, and all those with poster presentations. He also congratulated all the awardees who had conducted

world-class studies and proved themselves as leading experts in their research area. Finally, Dr Chui thanked the organising committee and all delegates for attending and looked forward to meeting them again at the next Health Research Symposium.

Risk of intracerebral haemorrhage in patients with cerebral microbleeds taking warfarin for atrial fibrillation: a prospective study

YO Soo *, J Abrigo, W Chu, KT Leung, WC Fong, SH Li, R Li, PW Ng, KK Wong, LKS Wong, TWH Leung

KEY MESSAGES

1. In Chinese patients with atrial fibrillation, the presence of ≥ 5 cerebral microbleeds on magnetic resonance imaging is associated with an increased risk of warfarin-related intracerebral haemorrhage.
2. Evaluation of cerebral microbleeds in patients with atrial fibrillation may help identify patients at higher risk of warfarin-related intracerebral haemorrhage, who may benefit from alternative treatment options with lower bleeding risk.

Hong Kong Med J 2019;25(Suppl 5):S6-8

HMRF project number: 01120136

¹ YO Soo, ² J Abrigo, ² W Chu, ¹ KT Leung, ³ WC Fong, ⁴ SH Li, ⁵ R Li, ⁶ PW Ng, ⁷ KK Wong, ¹ LKS Wong, ¹ TWH Leung

¹ Department of Medicine and Therapeutics, Prince of Wales Hospital, The Chinese University of Hong Kong

² Department of Imaging and Interventional Radiology, Prince of Wales Hospital, The Chinese University of Hong Kong

³ Department of Medicine, Queen Elizabeth Hospital

⁴ Department of Medicine, North District Hospital

⁵ Department of Medicine, Pamela Youde Nethersole Eastern Hospital

⁶ Department of Medicine and Geriatrics, United Christian Hospital

⁷ Department of Medicine, Yan Chai Hospital

* Principal applicant and corresponding author: yanniesoo@cuhk.edu.hk

Introduction

Atrial fibrillation (AF) is the most common cardiac arrhythmia worldwide. Irregular heartbeats can induce the formation of blood clots in the heart that dislodge and occlude arteries in the brain, accounting for a five-fold increase in the risk of ischaemic stroke. Oral anticoagulants can reduce the stroke risk in patients with AF by 68%. However, anticoagulant use is often limited by the potential risk of intracerebral haemorrhage (ICH). Over the past 15 years, there has been an almost three-fold increase in AF-related stroke in Hong Kong.¹

To optimise use of anticoagulants, better risk stratification of patients is needed for appropriate treatment. Cerebral microbleeds (CMBs) detected by magnetic resonance imaging are radiological markers that can predict future ICH.² CMBs are tiny old blood residues in brain, indicating previous silent mild leakage from fragile small vessels. CMBs are present in one-third of patients with AF³; this raises concerns about safety of anticoagulation in patients with CMBs, who may have higher risk of ICH that may outweigh the expected treatment benefit. A study explored whether CMBs could guide treatment decisions in AF,³ but the exact risk of ICH remains uncertain.

This prospective study aimed to evaluate the risk of ICH in Chinese patients taking warfarin for AF with concomitant CMBs.

Methods

This was a prospective multicentre observational study. Chinese patients who took warfarin for AF were recruited from eight public hospitals in Hong Kong. 3T magnetic resonance imaging (Achieva TX;

Philips Medical Systems, Best, Netherlands) was performed to evaluate CMBs. The standard stroke scanning protocol included 3D venous BOLD and axial FLAIR for detection of CMBs and white matter hyperintensities, respectively. A CMB was defined as an old, silent focus of signal loss in the susceptibility weighted imaging sequence, measuring 2 to 10 mm in diameter. White matter changes indicating underlying leukoaraiosis were visually rated using age-related white matter changes scale.

Primary outcome was ICH. Secondary outcomes were recurrent ischaemic stroke, systemic embolism, mortality of all causes, and mobility level. Patients were followed up for 2 years. Those with and without CMBs were compared.

Independent *t* test or non-parametric Mann-Whitney U test was used for comparison of continuous variables. The Chi-squared test was used for categorical variables. The Fisher's exact test was used when the expected count in any of the 2x2 table was < 5 . Multivariate regression model was used to determine predictors of ICH. Potential predictors were first tested using the univariate logistic regression model. Significant variables were further tested in the multivariate model using the stepwise-forward method and then adjusted by age. Statistical analyses were performed using SPSS (Windows version 24; IBM Corp, Armonk [NY], US). A P value of < 0.05 was considered statistically significant.

Results

Of 290 patients recruited, 53 were excluded based on pre-defined exclusion criteria and 237 were included in analysis. The mean follow-up period was 22.7 ± 10.2

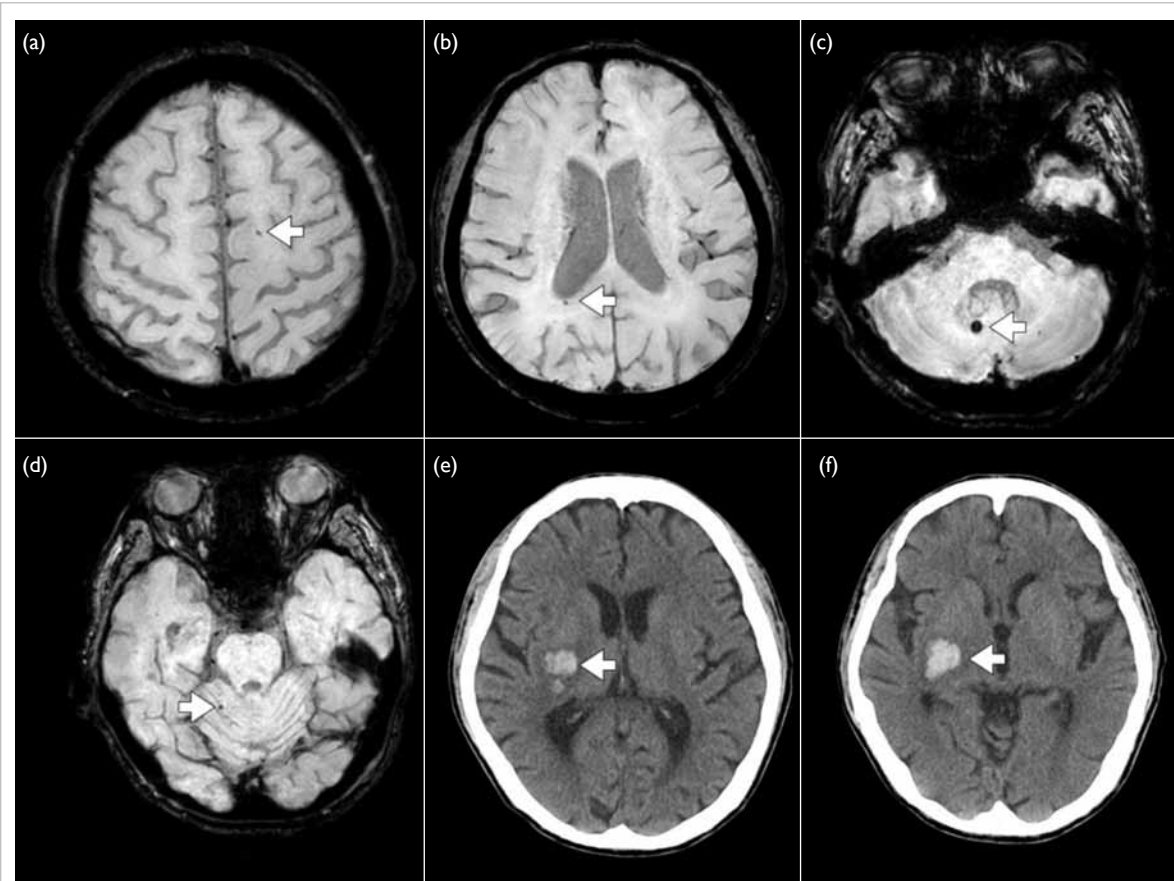


FIG. 68-year-old patient with a history of ischaemic stroke and atrial fibrillation treated with warfarin. Susceptibility-weighted magnetic resonance imaging of the brain at baseline showing a total of 5 cerebral microbleeds over the (a) left frontal lobe, (b) right parietal lobe, and (c, d) right cerebellum. (e, f) Computed tomography of the brain showing intracerebral haemorrhage over the right putamen region after the patient had sudden onset of left leg weakness 4 months after recruitment.

months.

CMBs were observed in 83 (35.0%) of patients. The mean number of CMBs was 3.1 ± 6.4 (range, 1-54); 9 (3.8%) patients had ≥ 5 CMBs (Fig). Patients with CMBs were more likely to have non-valvular AF, lower renal function level, and higher age-related white matter score. Those with and without CMBs were comparable in terms of the proportion of patients with a history of ischaemic stroke and other risk factors.

During the 2-year follow-up, there were more events of ischaemic stroke ($n=12$) and systemic embolism ($n=2$) than ICH ($n=4$) [Table 1]. Of the four patients with ICH, three had ≥ 5 CMBs and one had no CMB. Compared with patients without CMBs, patients with CMBs had a trend towards higher prevalence of ICH (3.6% vs 0.6%, $P=0.091$) and systemic embolism (2.4% vs 0%, $P=0.053$) at 2-year follow-up (Table 1). Compared with patients without ICH, patient with ICH were more likely to have underlying ischaemic heart disease or ≥ 5 CMBs (Table 2).

In multiple logistic regression, after adjusting for age, independent predictors for ICH were ≥ 5

TABLE 1. Comparison of outcomes in patients with and without cerebral microbleeds (CMBs) at 2-year follow-up*

	Total no. of events	Patients with CMBs (n=83)	Patients without CMBs (n=154)	P value
Intracerebral haemorrhage	4	3 (3.6)	1 (0.6)	0.091
Ischaemic stroke	12	6 (7.2)	6 (3.9)	0.264
Systemic embolism	2	2 (2.4)	0 (0.0)	0.053
Mortality of all causes	17	6 (7.2)	11 (7.1)	0.980
Modified Rankin Scale score	1.21 ± 1.94	1.3 ± 2.0	1.1 ± 1.9	0.412

* Data are presented as mean \pm standard deviation or No. (%) of patients

CMBs (odds ratio [OR]=18.53, 95% confidence interval [CI]=1.501-228.864, $P=0.023$) and ischaemic heart disease (OR=14.228, 95% CI=1.433-207.136, $P=0.025$).

Discussion

This is the first prospective study evaluating the risk of ICH in Chinese patients taking warfarin for AF with CMBs. A trend of higher prevalence of ICH at 2-year follow-up was observed in patients with CMBs. And

TABLE 2. Comparison of clinical and radiological outcomes in patients with and without intracerebral haemorrhage (ICH) at 2-year follow-up*

Outcome	Patients with ICH (n=4)	Patients without ICH (n=233)	P value
Clinical			
Age, y	71.0±8.8	71.9±8.8	0.933
Baseline modified Rankin Scale score	0.5±0.6	0.6±1.1	0.336
Male	2 (50.0)	138 (59.2)	0.710
Smoker	1 (25.0)	75 (32.2)	0.760
Drinker	1 (25.0)	29 (12.4)	0.454
Hypertension	3 (75.0)	190 (81.5)	0.739
Diabetes mellitus	2 (50.0)	84 (36.1)	0.565
Hyperlipidaemia	3 (75.0)	119 (51.1)	0.342
Congestive heart failure	1 (25.0)	51 (21.9)	0.881
Ischaemic heart disease	2 (50.0)	23 (9.9)	0.010
Newly diagnosed atrial fibrillation	1 (25.0)	29 (12.4)	0.454
Non-valvular atrial fibrillation	2 (100.0)	134 (86.5)	0.576
History of ischaemic stroke or transient ischaemic attack	3 (75.0)	128 (54.9)	0.424
History of ICH	0 (0.0)	1 (0.4)	0.896
Modification of diet in renal disease study equation	51.7±32.0	68.3±21.9	0.139
CHA2DS2-VASc (congestive heart failure, hypertension, age ≥75 years, diabetes mellitus, stroke/transient ischaemic attack/thrombo-embolism, vascular disease, age 65-74 years, sex category) score	5.3±2.2	4.2±1.6	0.224
HAS-BLED (hypertension, abnormal renal or liver function, stroke, bleeding, labile INRs, elderly (age >65 years), drugs and alcohol) score	3.0±1.8	2.7±1.1	0.586
Prior use of aspirin	1 (25.0)	11 (4.7)	0.067
Prior use of non-vitamin K antagonist oral anticoagulants	0 (0.0)	1 (0.4)	0.896
Time within therapeutic range (international normalised ratio of 2 to 3)	35.3±31.4	52.6±20.8	0.102
Patients with time within therapeutic range of <60%	3 (75.0)	147 (63.1)	0.624
Radiological			
Age-related white matter change	6.3±5.9	4.7±3.3	0.361
Patients with cerebral microbleeds (CMBs)	3 (75.0)	80 (34.3)	0.091
No. of CMBs	22.3±27.5	2.4±3.1	0.337
Patients with ≥5 CMBs	2 (50.0)	7 (3.0)	<0.001
Patients with pure lobar CMBs	0 (0.0)	37 (15.9)	0.386
Patients with pure deep CMBs	0 (0.0)	7 (3.0)	0.725
Patients with mixed lobar CMBs	2 (50.0)	21 (9.0)	0.006
Patients with infratentorial CMBs	2 (50.0)	30 (12.9)	0.031

* Data are presented as mean ± standard deviation or No. (%) of patients

the presence of ≥5 CMBs and ischaemic heart disease were independent predictors for ICH.

Patients with ≥5 CMBs had a higher risk of warfarin-related ICH (3.6%). This appears to offset its benefit in patients with low CHA2DS2-VASc (congestive heart failure, hypertension, age ≥75 years, diabetes mellitus, stroke/transient ischaemic attack/thrombo-embolism, vascular disease, age 65-74

years, sex category) score of 1 to 2, whose expected stroke risk is 1.3% to 2.2% per year.⁴ Nevertheless, patients with CMBs should not be excluded from anticoagulation as they are also at increased risk of thromboembolism as shown in our study. Alternative treatment option with non-vitamin K antagonist oral anticoagulants, which have 50% less ICH risk than warfarin, is a safer alternative. However, the risk of non-vitamin K antagonist oral anticoagulant-related ICH in patients with CMBs remains unknown. Further studies with larger sample size are needed before CMBs evaluation can be incorporated into clinical use. Meta-analysis of pooled patient data through international collaboration can increase the statistical power. Collaboration with The Microbleeds International Collaborative Network is underway to address this question.⁵

Conclusion

The presence of ≥5 CMBs is associated with an increased risk of warfarin-related ICH and thromboembolism in Chinese patients with AF.

Acknowledgements

This study was supported by the Health and Medical Research Fund, Food and Health Bureau, Hong Kong SAR Government (#01120136). We acknowledge Hong Kong Health Check in providing imaging support.

Some patients in this study have been used as controls in: Soo Y, Abrigo J, Leung KT, et al. Correlation of non-vitamin K antagonist oral anticoagulant exposure and cerebral microbleeds in Chinese patients with atrial fibrillation. *J Neurol Neurosurg Psychiatry* 2018;89:680-6.

Results of this study have been published in: Soo Y, Abrigo JM, Leung KT, et al. Risk of intracerebral haemorrhage in Chinese patients with atrial fibrillation on warfarin with cerebral microbleeds: the IPAAC-Warfarin study. *J Neurol Neurosurg Psychiatry* 2019;90:428-35.

References

- Soo Y, Chan N, Leung KT, et al. Age-specific trends of atrial fibrillation-related ischaemic stroke and transient ischaemic attack, anticoagulant use and risk factor profile in Chinese population: a 15-year study. *J Neurol Neurosurg Psychiatry* 2017;88:744-8.
- Greenberg SM, Nandigam RN, Delgado P, et al. Microbleeds versus macrobleeds: evidence for distinct entities. *Stroke* 2009;40:2382-6.
- Fisher M. MRI screening for chronic anticoagulation in atrial fibrillation. *Front Neurol* 2013;4:137.
- Lip GY, Frison L, Halperin JL, Lane DA. Identifying patients at high risk for stroke despite anticoagulation: a comparison of contemporary stroke risk stratification schemes in an anticoagulated atrial fibrillation cohort. *Stroke* 2010;41:2731-8.
- Microbleeds International Collaborative Network. Worldwide collaboration in the Microbleeds International Collaborative Network. *Lancet Neurol* 2016;15:1113-4.

Autonomic dysfunction as measured by Ewing battery test to predict poor outcome after acute ischaemic stroke

L Xiong, G Tian, HW Leung, XY Chen, WH Lin, TWH Leung, YO Soo, DYW Siu, LKS Wong

KEY MESSAGES

1. The severity of autonomic dysfunction as measured by Ewing battery test predicts poor functional outcome after acute ischaemic stroke.
2. Severe autonomic dysfunction may be related to worse dynamic cerebral autoregulation in affected side in patients with anterior circulation infarct.
3. Relatively severe autonomic dysfunction is associated with lower variation of blood pressure

in patients following acute ischaemic stroke.

Hong Kong Med J 2019;25(Suppl 5):S9-11

HMRF project number: 01120566

L Xiong, G Tian, HW Leung, XY Chen, WH Lin, TWH Leung, YO Soo, DYW Siu, LKS Wong

Department of Medicine & Therapeutics, The Chinese University of Hong Kong

* Principal applicant and corresponding author: ks-wong@cuhk.edu.hk

Introduction

Central autonomic dysfunction is commonly seen in patients with ischaemic stroke. Certain measures of autonomic function in ischaemic stroke are associated with an adverse prognosis. For example, decreased heart rate variability is an independent predictor of 1-year mortality in patients with first-ever acute ischaemic stroke.¹ Decreased heart rate variability also correlates with the severity of neurological deficits and disability 6 months after acute ischaemic stroke.² In addition, reduced baroreflex sensitivity in the acute phase of stroke is an independent predictor for all-cause mortality over a median 4-year follow-up.³ Thus, early diagnosis of autonomic dysfunction has prognostic and therapeutic implications in acute stroke. This study aimed to investigate whether the severity of autonomic dysfunction as measured by Ewing battery test can predict poor outcome after acute ischaemic stroke.

Methods

In this hospital-based prospective cohort study, consecutive ischaemic stroke patients within 7 days of symptom onset were recruited from acute stroke unit in Prince of Wales Hospital. Inclusion criteria were: age ≥ 18 years, cerebral ischaemic stroke detected on computed tomography or magnetic resonance imaging, National Institutes of Health Stroke Scale score of 4 to 10, presence of good temporal window, and written informed consent given. Exclusion criteria were: dementia, any clinically relevant arrhythmia on admission (including atrial fibrillation), any major concurrent

illness (including chronic obstructive pulmonary disease, renal failure, and malignancies), fever, hypoxia, alterations in consciousness, and any relevant haemodynamic compromise on admission.

Autonomic function tests were performed by an experienced senior technician according to the Ewing battery test⁴ with a Task Force Monitor system (CNSystems Medizintechnik AG Graz, Austria) to measure non-invasive continuous heart rate and blood pressure.

Parasympathetic tests

Valsalva manoeuvre

The participant was asked to exhale for 15 s while maintaining an expiratory pressure of 40 mm Hg. The manoeuvre was performed at least three times to maximise participant compliance and ensure reproducibility. The Valsalva ratio was an index of heart rate changes that occur during a Valsalva manoeuvre. The Valsalva ratio was taken as the maximum R-R interval in the 15 s following expiration divided by the minimum R-R interval.

Deep breathing

Respiratory sinus arrhythmia was assessed by taking six deep breaths per minute with slow inhalation and exhalation (5 s each) at a frequency of 0.1 Hz. Participants were given adequate rehearsal. The timed breathing was performed with the aid of verbal coaching and a time indicator. The response was taken as the mean of the differences between the maximum and minimum instantaneous heart rate for each cycle. A minimum of three breaths was required for inclusion.

The 30:15 ratio

This was performed by rising from the supine to a standing position. The 30:15 ratio was the R-R interval at the 30th beat divides by the R-R interval at the 15th beat immediately after standing.

Sympathetic tests

Orthostasis

Change in systolic blood pressure was calculated as the difference between the nadir systolic blood pressure immediately after standing and the mean systolic blood pressure for the 20 beats immediately prior to standing.

Sustained handgrip

The participant was asked to hold the handgrip with maximal grip and then hold 30% of the maximal grip for 5 minutes. Change in diastolic blood pressure was calculated as the difference between the maximal diastolic blood pressure before releasing the handgrip and the mean diastolic blood pressure for the 20 beats immediately prior to handgrip.

Ewing classification of autonomic failure

Results for each autonomic test were classified as normal, borderline, and abnormal. Patients were classified as normal (all tests normal or one borderline), early (one of the three heart rate tests

abnormal or two borderlines), definite (two or more heart rate tests abnormal), severe (two or more heart rate tests abnormal plus one or both blood pressure tests abnormal or both blood pressure tests borderline), and atypical (any other combination). The severity of autonomic dysfunction was dichotomised into severe (definite, severe or atypical) or minor (normal or early).

Data analysis

Demographic data (age, sex, and risk factors such as hypertension, diabetes, hyperlipidaemia, ischaemic heart disease, and smoking) of each patient were collected. At 3 months after stroke onset, the proportion of patients with poor outcome (defined as modified Rankin Scale score of 3 to 6) was calculated. Group differences were examined using the Chi squared test.

Results

Of 150 patients (mean age, 66.4±9.9 years; 70.7% men) recruited, 36 (24.0%) were classified as minor autonomic dysfunction and 114 (76.0%) as severe autonomic dysfunction. The two groups were comparable in terms of baseline characteristics and current drugs use (all P>0.05) [Table]. At month 3, more patients in the severe autonomic dysfunction group had poor functional outcome (32.5% vs 13.9%, P=0.031) [Table]. Crude odds ratio (OR)

TABLE. Baseline characteristics and functional outcome at 3 months in patients with acute stroke patients classified according to Ewing battery test*

	Total cohort (n=150)	Minor autonomic dysfunction (n=36)	Severe autonomic dysfunction (n=114)	P value
Baseline characteristic				
Sex, men:women	106:44	29:7	77:37	0.135
Age, y	66.4±9.9	63.6±11.2	67.2±9.3	0.058
Hypertension	93 (62.0)	21 (58.3)	72 (63.2)	0.315
Diabetes mellitus	51 (35.4)	12 (33.3)	39 (36.1)	0.763
Previous stroke	34 (22.7)	8 (22.2)	26 (22.8)	0.986
Ischaemic heart disease	15 (10.0)	5 (13.9)	10 (8.8)	0.279
Hyperlipidaemia	65 (43.3)	14 (38.9)	51 (44.7)	0.783
Current smoker	64 (42.7)	22 (61.1)	42 (36.8)	0.066
Current drinker	34 (22.7)	13 (36.1)	21 (18.4)	0.098
National Institutes of Health Stroke Scale score on admission	5.7±1.8	5.4±1.7	5.8±1.8	0.246
BI on admission	69.8±9.6	70.2±8.3	68.5±10.2	0.825
Systolic blood pressure	165.5±31.2	167.2±31.6	164.9±31.3	0.749
Diastolic blood pressure	88.9±18.4	94.2±20.4	87.3±17.6	0.097
Functional outcome at 3 months				
Modified Rankin Scale score of >2	42 (28.0)	5 (13.9)	37 (32.5)	0.031

* Data are presented as mean ± standard deviation or No. (%) of patients

of the association between severity of autonomic dysfunction and 3-month unfavourable functional outcome after acute ischaemic stroke was 2.979 (95% confidence interval [CI]=1.071-8.284, $P=0.036$). After adjusting for confounding factors (diabetes mellitus and ischaemic heart disease), the severity of autonomic dysfunction remained significantly associated with unfavourable outcome (OR=3.171, 95% CI=1.116-9.009, $P=0.030$).

Discussion

In accordance with previous studies, we found that autonomic dysfunction occurs in acute ischaemic stroke. About 76.0% acute ischaemic stroke patients were diagnosed as having severe autonomic dysfunction. Patients with atypical, definite, or severe autonomic dysfunction were more likely to have a poor modified Rankin Scale score at 3 months. Thus, severe autonomic dysfunction is related to poor outcome in patients with acute ischaemic stroke.

Autonomic imbalance predicts poor outcome after stroke. Decreased heart rate variability correlates with the severity of neurological deficits and disability at 6 months after acute ischaemic stroke.² Lower 24-hour standard deviation of all normal-to-normal R-R interval values on admission may predict an unfavourable rehabilitation outcome and dependency in post-stroke patients, despite hospital-based rehabilitation.⁵ In general, lower normal-to-normal R-R interval values are due to a shift in autonomic balance toward sympathetic dominance, not only as an effect of impaired parasympathetic function but also as a result of increased sympathetic activity. In the current study, autonomic function was assessed by the Ewing battery test rather than heart rate variability analysis, because the Ewing battery test has been extensively evaluated and represents a simple and accurate approach for quantification of cardiovascular autonomic function, even when performed by physicians without a specific cardiovascular

expertise. Furthermore, the severity of autonomic dysfunction can be determined according to the Ewing battery test, which may be more accurate than other assessment methods. Therefore, autonomic monitoring using this method may be useful in predicting long-term outcome after acute ischaemic stroke.

Conclusion

Severe autonomic dysfunction is related to an unfavourable functional outcome in patients with acute ischaemic stroke. Findings of our study may have important implications for the risk of adverse cardiovascular events and mortality rates in stroke survivors.

Acknowledgements

This study was supported by the Health and Medical Research Fund, Food and Health Bureau, Hong Kong SAR Government (#01120566). We thank The Chinese University of Hong Kong (Focused Investment Scheme B) and the Institute of Innovative Medicine, The Chinese University of Hong Kong.

References

1. Colivicchi F, Bassi A, Santini M, Caltagirone C. Cardiac autonomic derangement and arrhythmias in right-sided stroke with insular involvement. *Stroke* 2004;35:2094-8.
2. Korpelainen JT, Sotaniemi KA, Huikuri HV, Myllylä VV. Abnormal heart rate variability as a manifestation of autonomic dysfunction in hemispheric brain infarction. *Stroke* 1996;27:2059-63.
3. Robinson TG, Dawson SL, Eames PJ, Panerai RB, Potter JF. Cardiac baroreceptor sensitivity predicts long-term outcome after acute ischemic stroke. *Stroke* 2003;34:705-12.
4. Ewing DJ, Borseley DQ, Bellavere F, Clarke BF. Cardiac autonomic neuropathy in diabetes: comparison of measures of R-R interval variation. *Diabetologia* 1981;21:18-24.
5. Bassi A, Colivicchi F, Santini M, Caltagirone C. Cardiac autonomic dysfunction and functional outcome after ischaemic stroke. *Eur J Neurol* 2007;14:917-22.

Dedifferentiation-reprogrammed mesenchymal stem cells for neonates with hypoxic-ischaemic brain injury

FY Yang, XH Zhang, LL Tsang, HC Chan, XH Jiang *

KEY MESSAGES

1. Human umbilical cord-derived mesenchymal stem cells (hUC-MSCs) can be manipulated via neuronal differentiation and dedifferentiation *in vitro*.
2. Compared with naïve hUC-MSCs, dedifferentiated hUC-MSCs reveal distinguished stem cell phenotype such as enhanced cell survival, neuronal differentiation potential, and cell migration.
3. Local administration of hUC-MSCs or dedifferentiated hUC-MSCs significantly improves brain functional recovery in hypoxic-ischaemic encephalopathy rat model.
4. Compared with hUC-MSC, dedifferentiated hUC-MSCs exhibit stronger repair function, as demonstrated by more improved motor, learning, and memory abilities.

5. The enhanced therapeutic effects of dedifferentiated hUC-MSCs are attributed to enhanced neural protection and promotion of endogenous repair.

Hong Kong Med J 2019;25(Suppl 5):S12-6

HMRF project number: 01120056

^{1,2} FY Yang, ^{1,2,3} XH Zhang, ^{1,2} LL Tsang, ^{1,2,3,4} HC Chan, ^{1,2,4} XH Jiang

¹ Epithelial Cell Biology Research Centre, The Chinese University of Hong Kong

² School of Biomedical Sciences, Faculty of Medicine, The Chinese University of Hong Kong

³ Sichuan University-The Chinese University of Hong Kong Joint Laboratory for Reproductive Medicine, West China Second University Hospital, Chengdu, China

⁴ The Chinese University of Hong Kong, Shenzhen Research Institute, Shenzhen, China

* Principal applicant and corresponding author: xjiang@cuhk.edu.hk

Introduction

Traditional treatments for hypoxic-ischaemic encephalopathy (HIE) involve prevention of apoptosis, necrosis, and inflammation. Stem cell-based therapy has shown many benefits in animal models. However, low levels of mesenchymal stem cells (MSC) survival and differentiation *in vivo* greatly limit their therapeutic effects and clinical use. We have demonstrated that rat bone marrow-derived MSCs can be reprogrammed via neuronal differentiation and dedifferentiation with enhanced cell survival and differentiation in treating HIE in neonatal rats.¹ In this study, we expand dedifferentiation platform to human umbilical cord-derived MSCs (hUC-MSCs), which are promising cell source for HIE treatment, because many neonates experience an HIE insult around the time of birth. Hypoxia has been shown to stimulate MSC survival, proliferation, and stem cell potential.² Thus, hUC-MSCs derived from the hypoxic neonate may have a better therapeutic potential.³

Methods

We tested our hypothesis in both cell culture and neonatal HIE rat model. This study included two parts: (1) to characterise dedifferentiated hUC-MSCs and compare the phenotypic properties

(proliferation, cell survival, differentiation, migrative abilities, neurotrophic effects) of dedifferentiated hUC-MSCs (De-hUCMSCs) with unmanipulated hUC-MSCs *in vitro*, and (2) to evaluate the therapeutic efficacy of De-hUCMSCs and determine the mechanisms underlying the beneficial effects of De-hUCMSCs in a HIE rat model.

Results

Part 1

When subjected to the pre-induction medium followed by modified neural medium, hUC-MSCs rapidly underwent dramatic morphological changes. After 6 hours of neural induction, >95% of cells presented with neuron-like morphology. In contrast, withdrawal of modified neural medium rapidly reverted MSC-derived neuron-like cells back to mesenchymal morphology. We then used various cell functional analyses to characterise the De-hUCMSCs, which exhibited a survival advantage over undifferentiated hUC-MSCs when challenged with hydrogen peroxide (Fig 1a). Next, we examined the migratory ability of hUC-MSCs and De-hUCMSCs toward different kinds of growth factors. Both were seeded in the upper chamber of transwells while different growth factors were added to the lower chambers. The migratory ability

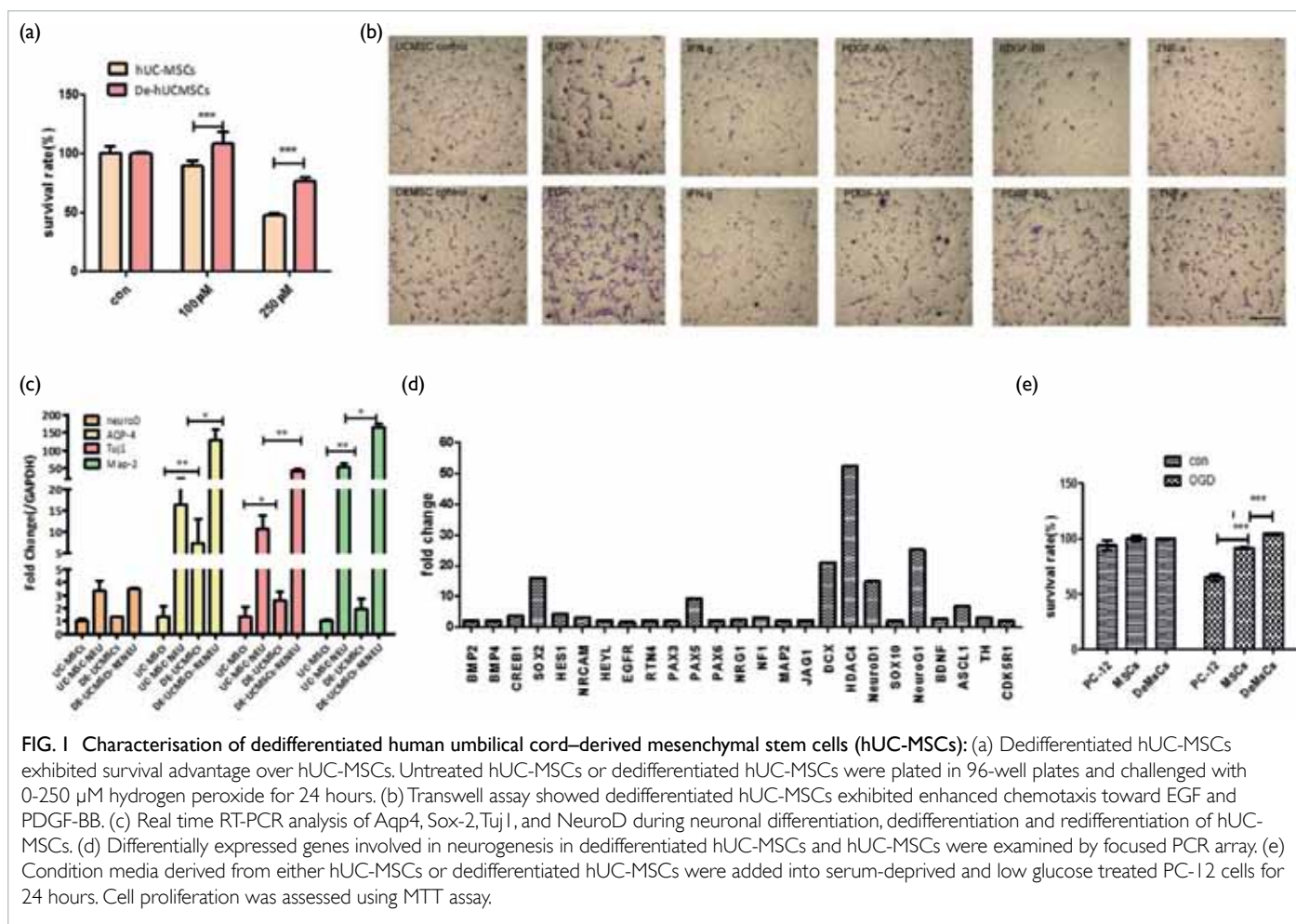


FIG. 1 Characterisation of dedifferentiated human umbilical cord-derived mesenchymal stem cells (hUC-MSCs): (a) Dedifferentiated hUC-MSCs exhibited survival advantage over hUC-MSCs. Untreated hUC-MSCs or dedifferentiated hUC-MSCs were plated in 96-well plates and challenged with 0–250 μ M hydrogen peroxide for 24 hours. (b) Transwell assay showed dedifferentiated hUC-MSCs exhibited enhanced chemotaxis toward EGF and PDGF-BB. (c) Real time RT-PCR analysis of Aqp4, Sox-2, Tuj1, and NeuroD during neuronal differentiation, dedifferentiation and redifferentiation of hUC-MSCs. (d) Differentially expressed genes involved in neurogenesis in dedifferentiated hUC-MSCs and hUC-MSCs were examined by focused PCR array. (e) Condition media derived from either hUC-MSCs or dedifferentiated hUC-MSCs were added into serum-deprived and low glucose treated PC-12 cells for 24 hours. Cell proliferation was assessed using MTT assay.

of hUC-MSCs was mildly enhanced in the presence of all growth factors, whereas De-hUCMSCs exhibited much enhanced chemotaxis to EGF and PDGFBB (Fig 1b). These findings suggest that the enhanced chemotaxis exhibited by De-hUCMSCs were specific to certain growth factors. In addition, we determined the neuronal differentiation and dedifferentiation at the molecular level. As shown by real time PCR analysis, the expression levels of Sox-2, NeuroD, Aqp4, Masashi-1, Tuj-1, and Map2 were markedly increased in differentiated cultures compared with undifferentiated hUC-MSCs. Dedifferentiation from the neuronal to the stem cell phenotype was associated with a marked reduction in the expression of neuronal proteins. However, the expression of Mashashi-1, Tuj-1, and Map2 in De-hUCMSCs was higher than that in undifferentiated hUC-MSCs, suggesting that De-hUCMSCs retained some neuronal traits. Indeed, De-hUCMSCs could undergo redifferentiation with full expression of the neuronal markers (Fig 1c). Next, various genes involved in neurogenesis were compared between hUC-MSCs and De-hUCMSCs using focused PCR array profiling. The expression of multiple

genes involved in neurogenesis were dramatically increased in De-hUCMSCs (Fig 1d), indicating a more potentiality of De-hUCMSCs towards neural fate. Furthermore, co-culture with either hUC-MSCs or De-hUCMSCs dramatically increased the number of viable cells after OGD, with significantly larger number of cells observed in co-culture with De-hUCMSCs as compared to that with hUC-MSCs (Fig 1e), indicating enhanced neuroprotective effects on PC-12.

Part 2 Treatment groups

A total of 134 adult Sprague Dawley rats were used. 24 rats were used in the preliminary experiment to establish the conditions of the rat HIE model. Ten rats were used to establish intracranial stem cell delivery method.

In the first experiment, 45 rats were divided into three groups (15 per group): phosphate-buffered saline (PBS), UC-MSCs, and De-hUCMSCs groups. 60–70% neonatal rats survived after HIE procedure. Three days after, stem cell treatment was

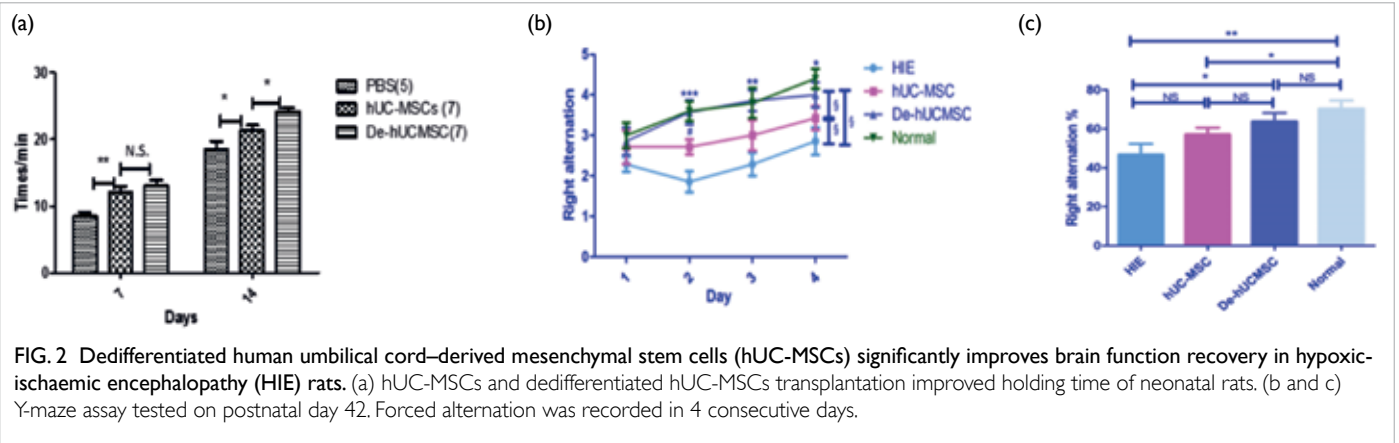


FIG. 2 Dedifferentiated human umbilical cord-derived mesenchymal stem cells (hUC-MSCs) significantly improves brain function recovery in hypoxic-ischaemic encephalopathy (HIE) rats. (a) hUC-MSCs and dedifferentiated hUC-MSCs transplantation improved holding time of neonatal rats. (b and c) Y-maze assay tested on postnatal day 42. Forced alternation was recorded in 4 consecutive days.

given intracranially to the survived neonatal rats. At day 6 after stem cell transplantation, rats were deeply anaesthetised, and the brain was fixed by trans-cardiac perfusion of 4% PFA. Fixed brain was embedded in OCT and 5-µm coronal sections were cut by cryostat. In the second experiment, 45 rats were used for behaviour tests (rotarod and shuttle box test) before and after stem cell transplantation. In the third batch of experiment, 10 neonatal rats were used for testing the feasibility of systemic injection of stem cells.

Functional outcomes

The sensorimotor cortex, striatum, and hippocampus of rats were predominantly damaged after HIE insult. Therefore, two corresponding behavioural tests were chosen; Y maze test was used for assessing spatial learning and memory for function of the hippocampus, and rotarod test for a motor cortical dysfunction.

In the rotarod test, the rats were given two attempts (5 minutes each) daily for 3 consecutive days of training. During the training period, the rotarod was set on an accelerating mode (from 4 to 20 rpm over 5 minutes), and this rotational speed was increased by 5 rpm each day. On day 3 of training, the rotational speed had reached 30 rpm, representing the speed used for the subsequent day’s challenge. At day 7 (11 days after stem cell treatment), rats were given two attempts, and the summed duration of on rod-holding was recorded. In comparison with PBS-treated animals, both hUC-MSC- and hDe-UCMSC-treated groups significantly increased holding time at day 7 (11 days after stem cell treatment), while transplantation of either hUC-MSCs or De-hUCMSCs appeared to increase the holding time, this effect was more pronounced in rats receiving De-hUCMSCs than hUC-MSCs. In addition, at day 14, De-hUCMSC-treated rats showed a better recovery compared to hUCMSC-

treated rats. (Fig 2a).

We then performed Y-maze with spontaneous and forced alternation in stem cell-transplanted HIE rats to measure their spatial working memory after they grew up (post-natal day 42). The percentage of alternation behaviours (both forced and spontaneous alternation) significantly decreased in HIE rats. This indicated that HIE mice developed working memory impairment. While hUC-MSC treatment slightly improved forced alternation behaviour, the alternation behaviour in De-hUCMSC-treated group was more significantly improved, in which almost recovered to a level equivalent to the normal group (Fig 2b, c). Altogether, these results indicated that De-hUCMSCs more effectively improved brain functional recovery in HIE.

Mechanistic studies

To determine the molecular mechanisms underlying the therapeutic effects of stem cells, rats were sacrificed and the brains were fixed by transcatheter perfusion of 4% PFA to perform immunofluorescent staining. The brain sections were stained with haematoxylin and eosin for evaluation of injured area. First, we sacrificed the rats 3 days after stem cell transplantation to determine whether hUC-MSCs or De-hUCMSCs could engraft into the injured area. Both hUC-MSCs (n=4) and De-hUCMSCs (n=5) engrafted into the injured area of the brain, there were no differences in the engraftment ability between two groups. Strikingly, both hUC-MSCs or De-hUCMSCs transplantation significantly decreased the injured lesion in the brain. However, there were no significant change between hUC-MSCs group or De-hUCMSCs group. We performed further immunofluorescent staining in the lesion boundary zone compared to the contra-side using neuron markers, such as MAP2, NeuN, and Nestin to evaluate the effect of stem cell treatment on neuronal protection in different groups

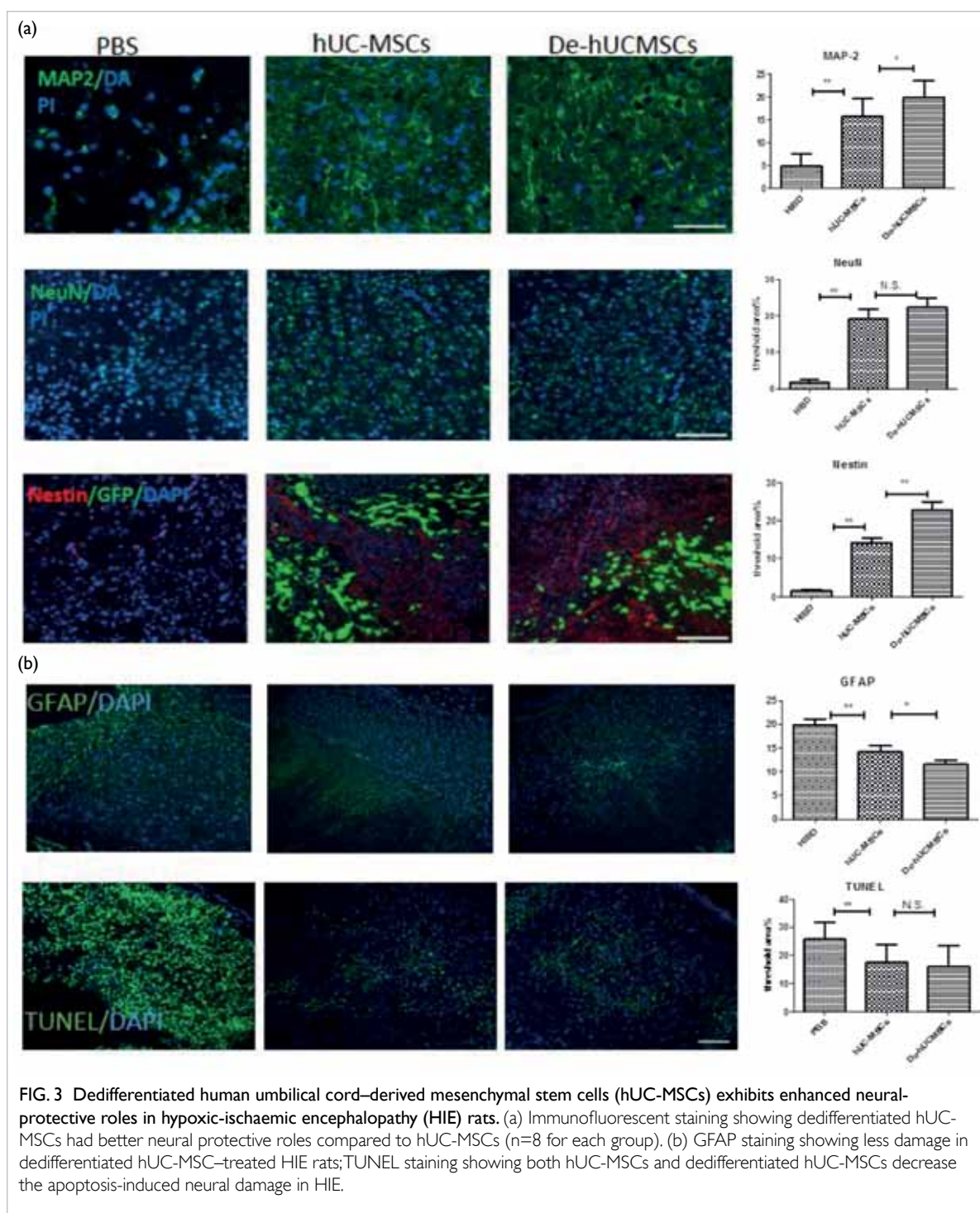


FIG. 3 Dedifferentiated human umbilical cord-derived mesenchymal stem cells (hUC-MSCs) exhibits enhanced neural-protective roles in hypoxic-ischaemic encephalopathy (HIE) rats. (a) Immunofluorescent staining showing dedifferentiated hUC-MSCs had better neural protective roles compared to hUC-MSCs (n=8 for each group). (b) GFAP staining showing less damage in dedifferentiated hUC-MSC-treated HIE rats; TUNEL staining showing both hUC-MSCs and dedifferentiated hUC-MSCs decrease the apoptosis-induced neural damage in HIE.

(Fig 3a). The expression of neuronal markers was dramatically increased with stem cell treatment. Of note, the expression of MAP2 and Nestin was more significantly increased in the De-hUCMSC-treated rats than in the hUC-MSC-treated rats, indicating De-hUCMSC with enhanced protective role in neuronal damage.

GFAP-staining was performed to identify reactive astrocytes in the brain after HIE. When

neurons are damaged by ischaemia, astrocytes will generate to fill the space of dead neurons. Thus, the expression level of GFAP indicates the degree of brain damage. HIE alone exhibited significantly increased percentage of GFAP⁺ cells in the lesion boundary zone of the injured hemisphere compared to contra-side. Stem cell treatment significantly reduced the GFAP⁺ astrocyte in the injured brain compared to the PBS treatment. However, the effect

of De-hUCMSC on reducing the GFAP⁺ astrocytes in the injured was more profound (Fig 3b). We then stained the brain tissues with TUNEL to evaluate the apoptotic response in untreated or stem cell-treated HIE models. Both hUC-MSCs and De-hUCMSCs treatment significantly decreased TUNEL positive cells compared to the PBS-treated group, indicating that stem cell treatment alleviated apoptosis-induced damage in HIE model (Fig 3b). However, there was no difference between hUC-MSCs and De-hUCMSCs treatment.

Conclusions

Local administration of hUC-MSCs or De-hUCMSCs significantly improved HIE recovery. Nonetheless, De-hUCMSCs exhibited stronger repair function than hUC-MSCs. Better functional recovery after treatment with De-hUCMSCs is associated with better neuronal protective roles. Although neither hUC-MSCs nor De-hUCMSCs express Nestin after engraftment, cells around them express extremely high levels of Nestin, suggesting that hUC-MSCs or De-hUCMSCs probably establish a niche benefit for endogenous stem cell regeneration in HIE brains. This effect is much stronger in De-hUCMSC-treated HIE brain. Altogether, De-hUCMSCs may elicit better therapeutic efficacy by paracrine effects on neuro-protection and neuro-regeneration.

With easy culture manipulation and low tendency of tumour formation, dedifferentiation strategy provides a feasible approach to enhance the therapeutic efficacy of stem cell therapy. De-

hUCMSCs could be a superior source of stem cells to treat HIE.

Acknowledgement

This study was supported by the Health and Medical Research Fund, Food and Health Bureau, Hong Kong SAR Government (#01120056).

Results from this study have been published in: (1) Chen R, Lee WY, Zhang XH, et al. Epigenetic modification of the CCL5/CCR1/ERK axis enhances glioma targeting in dedifferentiation-reprogrammed BMSCs. *Stem Cell Reports* 2017;8:743-57. (2) Zhang J, Weng ZH, Tsang KS, Tsang LL, Chan HC, Jiang XH. MycN is critical for the maintenance of human embryonic stem cell-derived neural crest stem cells. *PLoS One* 2016;11:e0148062. (3) Ke C, Biao H, Qiangian L, Yunwei S, Xiaohua J. Mesenchymal stem cell therapy for inflammatory bowel diseases: promise and challenge. *Curr Stem Cell Res Ther* 2015;10:499-508.

References

1. Liu Y, Jiang X, Zhang X, et al. Dedifferentiation-reprogrammed mesenchymal stem cells with improved therapeutic potential. *Stem Cells* 2011;29:2077-89.
2. Dos Santos F, Andrade PZ, Boura JS, Abecasis MM, da Silva CL, Cabral JM. Ex vivo expansion of human mesenchymal stem cells: a more effective cell proliferation kinetics and metabolism under hypoxia. *J Cell Physiol* 2010;223:27-35.
3. van Velthoven CT, Kavelaars A, van Bel F, Heijnen CJ. Mesenchymal stem cell transplantation changes the gene expression profile of the neonatal ischemic brain. *Brain Behav Immun* 2011;25:1342-8.

Topically applied adipose-derived mesenchymal stem cell treatment in experimental focal cerebral ischaemia

GKC Wong *, PK Lam, AWI Lo, AKY Chan, YX Wang, WS Poon

KEY MESSAGES

1. Topically applied mesenchymal stem cells plus fibrin sealant can home to ischaemic penumbra, reduce cerebral infarction volume, and improve the neurological function from cerebral ischaemia in a rodent middle carotid artery occlusion model mimicking severe stroke secondary to a major cerebral artery occlusion.
2. Topical mesenchymal stem cell plus fibrin sealant treatment is promising and should be optimised for safety and efficacy.

Hong Kong Med J 2019;25(Suppl 5):S17

HMRF project number: 01120666

^{1,2} GKC Wong, ^{1,2} PK Lam, ³ AWI Lo, ³ AKY Chan, ⁴ YX Wang, ^{1,2} WS Poon

¹ Department of Surgery, The Chinese University of Hong Kong

² Chow Tai Fook-Cheng Yu Tung Surgical Stem Cell Research Center, The Chinese University of Hong Kong

³ Department of Anatomical Pathology, Queen Mary Hospital

⁴ Department of Imaging and Interventional Radiology, The Chinese University of Hong Kong

* Principal applicant and corresponding author:
georgewong@surgery.cuhk.edu.hk

Introduction

Stroke is the third most common cause of death in developed countries after ischaemic heart disease and malignancy, and the fourth most common cause of death in Hong Kong. Despite prophylactic decompressive craniectomy after hemispheric infarction (typically middle cerebral artery infarction), the rates of death and disability remain high. In the micro-environment, mesenchymal stem cells (MSCs) suppress inflammation and apoptosis, enhance angiogenesis, and stimulate proliferation and cellular differentiation. Experimental and pilot clinical studies have reported the board therapeutic effects of MSCs in various neurological disorders including cerebral ischaemic injury.¹⁻³

Topical application is an efficient delivery of MSCs to the brain. Theoretically billions of MSCs in a single topical transplantation can be readily applied to the surface of human cerebral cortex without causing additional injury to the brain or related complications. This study aimed to investigate the engraftment and underlying mechanism of topically applied adipose-derived MSCs in experimental cerebral ischaemia, and to assess the neuroprotective effects.

Methods

A rat focal cerebral ischaemia model was used. At 24 hours after experimental focal cerebral ischaemia, 120 rats were randomised to three groups: topical application of MSCs plus fibrin (n=40), topical application of MSCs alone (n=40), and no treatment (n=40). Radiological and histological assessment of cerebral infarction, neurological assessments, microscopic assessments, and expression of

inflammatory cytokines were performed.

Results

Topically applied MSCs plus fibrin sealant homed to the ischaemic penumbra, reduced cerebral infarction volume, and improved the neurological function from cerebral ischaemia. However, these effects could not be explained by suppression of inflammation and apoptosis in the ischaemic penumbra.

Conclusion

Topical MSC plus fibrin sealant treatment is promising and should be optimised for safety and efficacy in severe stroke secondary to major cerebral artery occlusion.

Acknowledgements

This study was supported by the Health and Medical Research Fund, Food and Health Bureau, Hong Kong SAR Government (#01120666) and the Chow Tai Fook-Cheng Yu Tung Surgical Stem Cell Research Centre of The Chinese University of Hong Kong.

References

1. Joyce N, Annett G, Wirthin L, Olson S, Bauer G, Nolta JA. Mesenchymal stem cells for the treatment of neurodegenerative disease. *Regen Med* 2010;5:933-46.
2. Bliss TM, Andres RH, Steinberg GK. Optimizing the success of cell transplantation therapy for stroke. *Neurobiol Dis* 2010;37:275-83.
3. Keimpema E, Fokkens MR, Nagy Z, et al. Early transient presence of implanted bone marrow stem cells reduces lesion size after cerebral ischaemia in adult rats. *Neuropathol Appl Neurobiol* 2009;35:89-102.

Effects of collateral circulation on haemodynamic flow status in intracranial artery stenosis depicted by computational fluid dynamics

TWH Leung *, SY Fan, HL Ip, AYL Lau, DYW Siu, EYL Dai, LKS Wong, DS Liebeskind

KEY MESSAGES

1. Risk of stroke recurrence is not solely affected by the degree of anatomical stenosis.
2. Haemodynamic changes across the stenosed vessel are as important as the degree of luminal narrowing in terms of implication on stroke risk.
3. Studying haemodynamic changes in the cerebral circulation is feasible with computational fluid dynamics technique coupling to various imaging modalities, including computed tomographic angiography.

Hong Kong Med J 2019;25(Suppl 5):S18-21

HMRP project number: 01120466

TWH Leung, SY Fan, HL Ip, AYL Lau, DYW Siu, EYL Dai, LKS Wong, DS Liebeskind

Division of Neurology, Department of Medicine and Therapeutics, The Chinese University of Hong Kong

* Principal applicant and corresponding author: drtleung@cuhk.edu.hk

Introduction

Intracranial atherosclerotic steno-occlusive disease (ICAS) is a major cause of stroke. Stroke results in significant morbidity and mortality. In Hong Kong, stroke has been the commonest cause of permanent disability in adulthood and the fourth leading cause of death in the past 10 years. Although there are a lot of studies on effective means to reduce stroke incidence and improve stroke outcome in ICAS, remarkable progress is yet to be seen. One key element of successful intervention is to identify patients most vulnerable to stroke relapse and in need of timely adjunctive treatments.

In ICAS, the degree of arterial stenosis is predictive of stroke risk. In the Warfarin-Aspirin Symptomatic Intracranial Disease trial, the 1-year stroke risk for patients with symptomatic ICAS of $\geq 70\%$ was up to 18%. Yet, emerging evidence showed that the degree of arterial stenosis may not be the only factor governing stroke risk. Other factors, particularly those that impact on the haemodynamics across ICAS, including the extent of collateralisation¹ and plaque morphology, may play a role.

The novel technique of computational fluid dynamics (CFD), coupled with various angiographic modalities, enables assessment of haemodynamics in the cerebral circulation.

We aimed to measure the haemodynamic parameters of a symptomatic high-grade intracranial stenosis in a CFD model derived from computed tomographic angiography (CTA), and correlated these factors to the extent of collateralisation as depicted by digital subtraction angiography (DSA) in patients with symptomatic ICAS. We aimed to

explore the feasibility and potential of coupling of CFD technique to CTA as a non-invasive means to assess anatomical and functional severity of ICAS.

Methods

We recruited patients from the neurovascular intervention registry in the Division of Neurology, Department of Medicine and Therapeutics, Prince of Wales Hospital from November 2006 to June 2012. These ischaemic stroke patients were aged 18 to 80 years and underwent both DSA and CTA within 1 month of stroke as part of vascular workup. Patients were eligible if DSA confirmed a stenotic lesion of $\geq 50\%$ in a relevant intracranial large artery. Patients were excluded if they had (1) suspected non-atherosclerotic ICAS such as vasculitis, dissections or Moya-Moya disease, (2) suspected cardioembolic stroke, (3) prior intervention or surgical procedures in intra- or extra-cranial ICAS, or (4) DSA or CTA examinations performed in other hospitals where source data could not be retrieved.

We recorded the baseline demographics, neurological status, and risk factor profile of the patients. These included gender, age, blood pressure, fasting blood glucose level, glycosylated haemoglobin level and lipid profile on presentation; prior medical history of diabetes mellitus, dyslipidaemia, prior history of ischaemic heart disease and peripheral vascular disease, prior history of stroke and transient ischaemic attacks, smoking and drinking history, baseline NIH Stroke Scale and modified Rankin score on presentation.

Relevant arterial stenosis on DSA was measured based on the Warfarin-Aspirin

Symptomatic Intracranial Disease Trial. The extent of collateralisation was assessed based on the American Society of Interventional and Therapeutic Neuroradiology collateral flow grading system.² Grade 0 or 1 is regarded as poor collateral flow, and grade 2 or above is regarded as good collateral flow.

The arterial segment with the relevant symptomatic ICAS was visually identified and selected on CTA images. The source images were used for construction of simulated model using commercially available software and programs, including ANSYS ICEM-CFD (ANSYS Inc), ANSYS CFX software, and Cray CX1 cluster (Cray Inc) program.

Simulated models were analysed using CFD techniques. The ANSYS CFX-post software was used for extraction and evaluation of haemodynamic parameters. For each symptomatic ICAS, haemodynamic parameters across the lesion were evaluated, including pressure difference, pressure ratio, pressure gradient, shear strain rate (SSR) ratio, wall shear stress (WSS) ratio, and velocity ratio (Fig).

The baseline demographics and risk factors were summarised with their means and prevalence in the cohort presented. For modified Rankin score and National Institute of Health Stroke Score

were non-parametric variables and thus median and interquartile ranges were presented. The haemodynamic parameters demonstrated skewed distribution upon testing for normality with the Kolmogorov-Smirnov test, so their median and interquartile ranges were presented. Spearman's correlation test was used to explore the correlation between the haemodynamic parameters and the extent of collateralisation. Two-sided P values of <0.05 were considered statistically significant. Linear regression technique was used to adjust for the effects of age, blood pressure, and glucose level.

Results

A total of 55 patients were recruited. Three patients had outlying values in the haemodynamic parameters in the post-processed CFD models and were excluded from analysis. The demographic characteristics and risk factor profiles of the remaining 52 patients are shown in Table 1.

The mean of arterial stenosis was 75.1%. 46 (88.5%) patients had ICAS in anterior circulation; four lesions were in internal carotid arteries and 42 lesions were in middle cerebral arteries. Six patients had ICAS over intracranial segments of

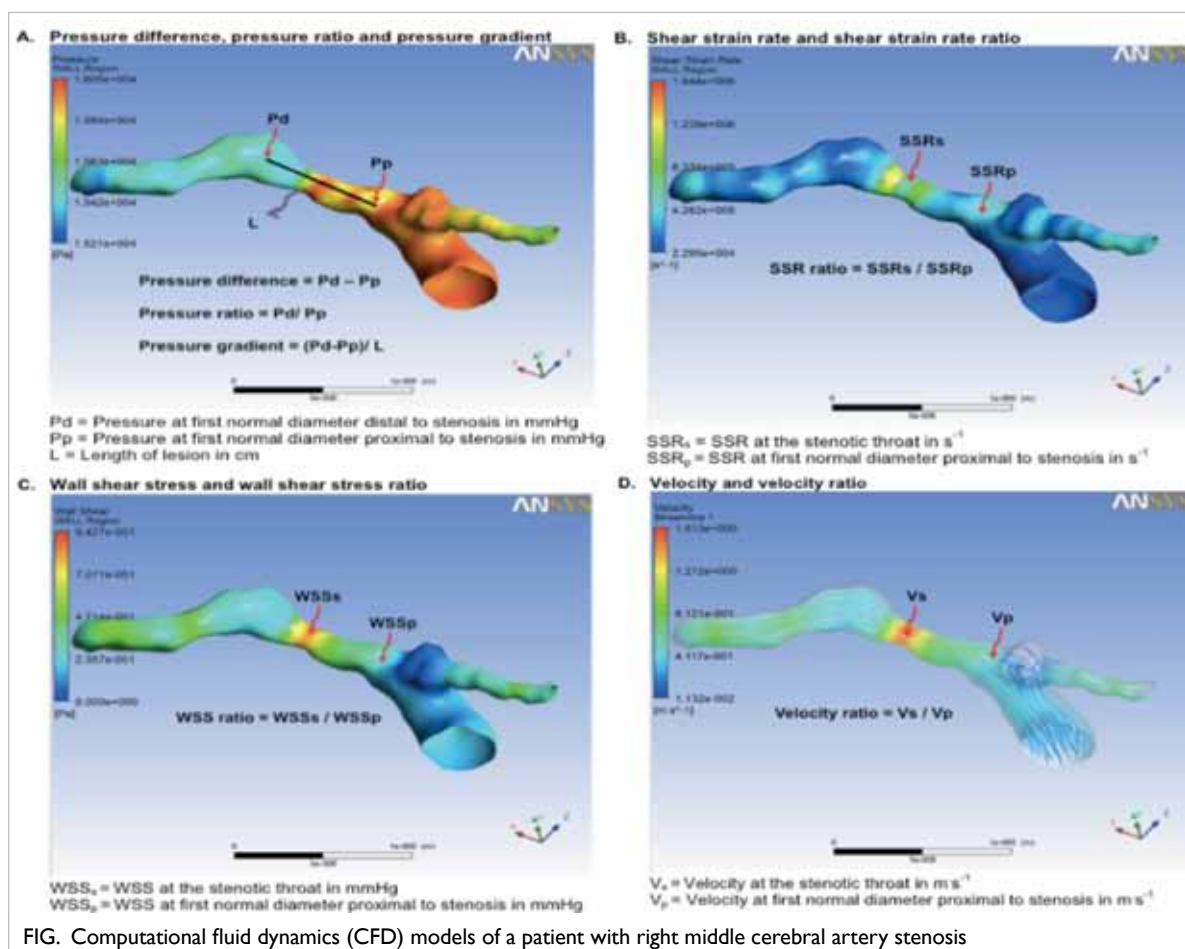


FIG. Computational fluid dynamics (CFD) models of a patient with right middle cerebral artery stenosis

vertebrobasilar arteries.

The extent of collateralisation showed weak but significant correlations with pressure difference ($r_s = -0.28, P=0.04$), pressure ratio ($r_s=0.31, P=0.03$), and pressure gradient ($r_s= -0.29, P=0.03$) [Table 2]. After adjustments for age, blood pressure, and glucose level, the correlations became insignificant. No correlation was found with SSR ratio, WSS ratio, or velocity ratio, or among patients with symptomatic lesions in anterior circulation or

posterior circulation, or with moderate (50%-69% stenosis) or severe (70%-99% stenosis) ICAS.

Discussion

Pressure ratio and pressure gradients reflect the more ‘static’ aspect of the haemodynamics across ICAS, whereas the SSR ratio, WSS ratio, and velocity ratio reflect the more ‘dynamic’ aspect of it. Shear strain rate of blood flow reflects the spatial gradient of flow velocity. To understand such concept, the blood volume inside the vessel should be considered as many thin layers of blood flow. SSR refers to the relative changes of flow velocity between these infinitesimally thin layers of blood flow. Turbulent flow at the stenotic throat increases the relative flow velocities between the layers and leads to increased SSR. WSS of blood flow reflects flow induced stress and can be conceptualised as frictional force of viscous blood. Turbulent blood flow across the stenotic lesion increases the wall shear stress. Therefore, the ratio of SSR, WSS, and velocity at the stenotic throat and the proximal normal segment of vessel were examined to reflect the haemodynamic changes.

From our study, the extent of collateralisation showed weak correlation with pressure difference, pressure ratio, and pressure gradient, such correlation became insignificant after adjustments for age, blood pressure, and glucose level. There were no correlations with SSR ratio, WSS ratio, and velocity ratio.

The presence of multiple cardiovascular risk factors (hypertension, diabetes, and hyperlipidaemia) promotes the formation of an atherosclerotic plaque in a vessel. Plaque formation results in narrowing of the vessel lumen and disturbs the normal laminar blood flow. During an acute ischaemic event, blood flow across the diseased vessel is disturbed and reduced, leading to a pressure drop downstream. Such a pressure drop leads to collateral circulation by

TABLE 1. Baseline demographics of 52 patient

Characteristic	Value*
Age, y	63.2±10.5
Male	37 (67.3)
History of hypertension	40 (76.9)
History of diabetes mellitus	17 (32.7)
History of hyperlipidaemia	48 (92.3)
History of ischaemic heart disease or peripheral vascular disease	0
History of stroke or transient ischaemic attack	13 (25)
Smoking history	21 (40.4)
Drinking history	7 (13.5)
National Institute of Health Stroke score	2 (1-3)
Modified Rankin score	1 (1-2)
Systolic blood pressure, mmHg	162.6±25.6
Diastolic blood pressure, mmHg	86.8±15.2
Low density lipoprotein-cholesterol, mmol/L	3.6±1.1
Triglycerides, mmol/L	1.5±0.7
High density lipoprotein-cholesterol, mmol/L	1.2±0.3
Fasting glucose, mmol/L	6.5±2.5
Glycated haemoglobin, %	6.4±1.6

* Data are presented as mean ± standard deviation, No. (%) of patients, or median (range)

TABLE 2. Correlations between the extent of collateralisation and various haemodynamic parameters

	Correlations between the extent of collateralisation and											
	Pressure difference		Pressure ratio		Pressure gradient		Shear strain rate ratio		Wall shear stress ratio		Velocity ratio	
	r_s	P value	r_s	P value	r_s	P value	r_s	P value	r_s	P value	r_s	P value
Entire cohort	-0.28	0.04	0.31	0.03	-0.29	0.03	-0.01	0.95	-0.13	0.37	-0.17	0.24
Entire cohort (adjusted for age, blood pressure and glucose level)	-0.11	0.49	0.11	0.46	-0.17	0.26	-0.16	0.28	-0.05	0.73	-0.12	0.41
Anterior circulation stroke/transient ischaemic attack	-0.22	0.14	0.25	0.1	-0.24	0.1	0.03	0.85	-0.14	0.36	-0.12	0.42
Posterior circulation stroke/transient ischaemic attack	-0.62	0.19	0.62	0.19	-0.63	0.18	-0.21	0.69	-0.41	0.41	-0.62	0.19
50%-69% stenosis	-0.25	0.36	0.31	0.24	-0.16	0.54	-0.53*	0.03	-0.16	0.54	-0.29	0.28
70%-99% stenosis	0.11	0.53	-0.12	0.51	0.08	0.63	0.14	0.42	0.04	0.81	0.12	0.48

activating the endothelium and stimulating a cascade of signalling events, involving a number of cytokines release and inflammatory cells. The process was known as arteriogenesis.³ Such process can occur within hours of an acute event and remain active weeks to months afterwards. The interplay between collateral flow and arterial occlusion is complicated. Study correlating collateral flow status with the haemodynamics across ICAS was scarce and yielded conflicting results. On the one hand, in an acute event, good collateral circulation was associated with less severe stroke and better stroke outcome. It was also associated with better clinical response and lower rate of haemorrhagic transformation during thrombolysis and recanalisation therapies. On the other hand, in patients with chronic arterial stenosis, the recruitment of collateral flow often signifies severe stenotic lesions compromising flow downstream, therefore implying higher risk of stroke. Thus, the age of the lesion and the timing of imaging of collateral flow impact on the assessment and interpretation of the effect of collateral flow on haemodynamics across ICAS. This may contribute to the largely negative findings in our current study.

CTA is a useful tool for anatomical and functional assessments of ICAS when coupled to CFD techniques. Being non-invasive and more widely available, it is more acceptable by patients, physicians, and researchers in the field to investigate the hidden haemodynamic aspect of ICAS. More studies are needed to determine the effect of

collateralisation on haemodynamics of ICAS, the correlation between different haemodynamic parameters and risk of recurrent stroke and clinical outcome. This may revolutionise and rationalise our management on stroke patients in the near future. With better understanding on the haemodynamic characteristics in ICAS, selection of patients with high risk of stroke recurrence for more aggressive treatments could be facilitated. The financial and social burdens of stroke could thus be minimised.

Acknowledgements

This study was supported by the Health and Medical Research Fund, Food and Health Bureau, Hong Kong SAR Government (#01120466). We thank the hard work and dedicated support from the medical and research teams of the Division of Neurology, Department of Medicine and Therapeutics, The Chinese University of Hong Kong.

References

1. Liebeskind DS, Cotsonis GA, Saver JL, et al. Collaterals dramatically alter stroke risk in intracranial atherosclerosis. *Ann Neurol* 2011;69:963-74.
2. Zaidat OO, Yoo AJ, Khatri P, et al. Recommendations on angiographic revascularization grading standards for acute ischemic stroke: a consensus statement. *Stroke* 2013;44:2650-63.
3. Liu J, Wang Y, Akamatsu Y, et al. Vascular remodeling after ischemic stroke: mechanisms and therapeutic potentials. *Prog Neurobiol* 2014;115:138-56.

Neutralising antibodies to interferon-beta therapy in relapsing multiple sclerosis: a pilot study

AYL Lau *, E Chan, KK Lau, V Mok, DYW Siu, R Lee

KEY MESSAGES

1. In a cohort of Chinese patients with multiple sclerosis who received interferon-beta for ≥ 9 months, binding antibodies to interferon-beta was found in 78% of patients, whereas neutralising antibodies (NAB) were found in 28% of patients, based on an ELISA-based MxA protein induction assay.
2. Patients with NAB are six times more likely to respond poorly to interferon-beta, as evidenced by multiple relapses and extensive activity on magnetic resonance imaging.
3. MxA gene induction and protein induction assays are reliable screening and confirmatory tests for NAB.

4. Routine testing for NAB should be implemented for Chinese patients with multiple sclerosis to identify poor responders early.

Hong Kong Med J 2019;25(Suppl 5):S22-5

HMRF project number: 01120486

¹ AYL Lau, ² E Chan, ³ KK Lau, ¹ V Mok, ⁴ DYW Siu, ⁴ R Lee

¹ Department of Medicine and Therapeutics, The Chinese University of Hong Kong

² Department of Pathology, Queen Mary Hospital

³ Department of Medicine, Princess Margaret Hospital

⁴ Department of Imaging and Interventional Radiology, Prince of Wales Hospital

* Principal applicant and corresponding author: alexlau@cuhk.edu.hk

Introduction

Multiple sclerosis (MS) is a disabling neurological disease affecting the central nervous system of young adults, and is the most common autoimmune inflammatory demyelinating disease worldwide.¹ Its prevalence in Hong Kong has risen by 40% from 4.8 per 100,000 persons in 2008 to 6.8 per 100,000 persons in 2015. Relapsing-remitting MS is the commonest presentation accounting for 80% of patients. For these patients, interferon-beta (IFN-beta) therapy remains the efficacious first-line treatment by reducing relapses, disability, and magnetic resonance imaging (MRI) disease burden. Up to 30% of patients with MS treated with IFN-beta may develop neutralising antibodies (NABs) to IFN-beta, which are associated with reduced treatment efficacy, disease relapse and progression.² Patients with persistent NABs and poor clinical response are recommended to switch to other disease-modifying treatment in most practice guidelines.²

To date there is no study on anti-IFN-beta and NAB in Chinese. We performed a cross-sectional study with an aim to develop and validate in-house assays to investigate the prevalence of anti-IFN-beta and neutralising antibodies among Chinese patients, and to study the association between NAB and clinical-radiological treatment response.

Methods

We recruited Chinese patients (aged ≥ 18 years)

with relapsing multiple sclerosis who received IFN-beta (1a or 1b) for ≥ 9 months and evaluated the clinical response in terms of relapse and lesion progressions on MRI. All patients gave written informed consent. A standard proforma was used to collect data of demographics, relapse, functions (assessed by the Expanded Disability Status Scale by neurologists), type, dosage, route of administration, duration of IFN-beta and other disease-modifying treatments, diagnosis, and relapses. The presence of new T2-hyperintense lesions, contrast-enhancing lesions, and enlarging lesions was assessed using MRI by radiologists. The clinical status of patients was assessed by neurologists in terms of overall response to IFN-beta as: (1) doing well: no relapses, no or limited MRI activity, (2) intermediate disease activity: one relapse during therapy, no or limited MRI activity, and (3) doing poorly: one or multiple relapses and extensive MRI activity.

The sample size was estimated to be 80 by convenience sampling. Blood was collected for isolation of serum and total RNA extraction. RNA was extracted from collected blood samples for relative gene expression of myxovirus resistance protein (MxA). Total RNA extracted from PBMC or PAXgene blood were converted to cDNA and then by qRT-PCR assay for MxA protein relative gene expression analysis. Sera were tested for IFN-beta binding antibodies (BAB), and NABs by MxA gene induction assay and protein induction assay. Luciferase reporter gene assay and cytopathic effect

assay were used as internal and external reference, respectively. Assay performances were evaluated by receiver operating characteristic curve (ROC) analysis. Statistical analyses were performed using SPSS (version 22.0, IBM) and GraphPad Prism 5.03. A two-tailed P value of <0.05 was considered statistically significant.

Results

We evaluated 78 patients (62 female) with MS using IFN-beta for ≥9 months from 10 hospitals in Hong Kong (Table 1). Their median age was 35 years (interquartile range [IQR], 27-45 years). The mean disease duration was 5.2±4.2 years. The mean neurological disability (measured by the Expanded Disability Status Scale) was 2.0 (range, 1.0-3.0), indicating mild disability. The mean duration of IFN-beta use was 3.7±2.9 years. The most commonly used IFN-beta was IFN-beta-1a SC (Rebif, n=52, 67%), followed by IFN-beta-1b SC (Betaferon, n=15, 19%), and IFN-beta-1a IM (Avonex, n=11, 14%). The most common clinical status was doing well (n=48, 62%), followed by doing poorly (n=21, 27%) and intermediate disease activity (n=9, 11%).

TABLE 1. Characteristics of 78 patients with relapsing multiple sclerosis receiving interferon-beta

Characteristic	Value
Age, y	36.0±9.9; 35 (27-45)
Female	62 (80)
Disease duration, y	5.2±4.2
Interferon use duration, y	3.7±2.9
Expanded Disability Status Scale score	2.0 (1-3)
Type of interferon used	
Interferon-beta-1a SC (Rebif)	52 (67)
Interferon-beta 1a IM (Avonex)	11 (14)
Interferon-beta-1b SC (Betaferon)	15 (19)
Clinical status	
Doing well	48 (62)
Intermediate disease activity	9 (11)
Doing poorly	21 (27)
Presence of binding antibodies	61 (78)
Presence of neutralising antibodies	
Luciferase assay	
20-100 TRU/mL	1 (1.3)
>100 TRU/mL	9 (11.5)
ELISA-based MxA protein induction assay	22 (28.2)
20-100 TRU/mL	12 (15.4)
>100 TRU/mL	10 (12.8)

* Data are presented as mean ± standard deviation, median (interquartile range), or No. (%) of patients

BAB was found in 61 (79%) patients who tended to be older (36.7 vs. 31.6 years, P=0.07), had higher Expanded Disability Status Scale score (2.1 vs. 1.3, P=0.06), and used IFN-beta for a longer duration (4.0 vs. 2.6 years, P=0.07). NAB was present in 22 (28.2%) patients. The titre was between 20 and 100, with tenfold reduction unit (TRU)/mL in 12 (15.4%) patients and >100 TRU/mL in 10 (12.8%) patients. Among various types of IFN-beta, NAB was present in 16/52 (31%) patients using Rebif (IFN-beta-1a SC), 2/11(18%) patients using Avonex (IFN-beta 1a IM), and 4/15 (27%) patients using Betaferon (IFN-beta-1b SC). The presence of NAB was not associated with age, gender, disease duration, types or duration of IFN-beta use (Table 2). However, the presence of NAB was associated with a higher number of clinical relapses after IFN-beta use (1.9 vs. 0.6, P=0.01) and poor clinical response (46% vs. 20%, P=0.03). In univariate analysis, patients with high titre NAB (>100 TRU/mL) were six times more likely to have poor outcome (odds ratio=6.3, 95% confidence interval=1.5-26.1, P=0.012). Nonetheless, no significant prediction was noted for intermediate NAB titre (TRU 20-100/mL) [odds ratio=2.4, 95% confidence interval=0.51-9.9, P=0.24]. Relative MxA gene expression was significantly lower (0.13 vs. 0.40, P<0.01) in NAB-positive patients than in NAB-negative patients (P<0.01) using high titre cut-off of 100 TRU/mL.

Twelve (15%) samples were sent to Mayo clinic for external validation by cytopathic effect assay. For MxA protein induction assay, the concordance was 67% (8/12) for a lower titre cut-off (>20 TRU/mL) and 100% when using a high titre cut-off (>100 TRU/mL).

ROC analysis was performed for relative MxA gene expression assay, BAB ELISA, and NAB by MxA induction assay (Fig). For BAB, using ELISA-based MxA protein induction assay (titre >100 TRU/mL) to define the presence of NAB, the area under curve (AUC) was 0.81. At the clinical cut-off of 30 BTU, the sensitivity was 100% and specificity was 38%. For relative MxA gene expression assay and NAB (MxA protein induction assay >100 TRU/mL), the AUC was 0.79. At a cut-off of 0.20, the sensitivity was 90% and the specificity was 64%. MxA gene expression has a better performance as a screening assay when compared to BAB ELISA.

Using luciferase assay as internal reference benchmark for the presence of NAB, the ROC of NABs levels between luciferase assay and ELISA-based MxA induction assay had AUC of 0.92 (Fig). At a cut-off of 20 TRU/mL, the sensitivity was 90% and specificity was 83%. At a cut-off of 100 TRU/mL, the sensitivity was 90% and specificity was 88%. For external validation using Mayo Clinic CPE assay, our in-house MxA protein induction assay had 67% (8/12) concordant results low titre cut-off (20

TABLE 2. Association between clinical predictors and presence of neutralising antibodies (NAB) by MxA protein induction assay

	NAB positive (n=22)	NAB negative (n=56)	P value
Age, y	35.8±10.1	35.5±10.5	0.90
Expanded Disability Status Scale score	2.3±1.5	1.8±1.4	0.24
Disease duration, y	4.6±4.4	5.4±4.3	0.48
Duration of interferon use, y	3.2±3.0	3.9±3.1	0.38
Female	16 (73)	46 (82)	0.37
Types of Interferon used			0.68
Rebif	16 (73)	36 (64)	
Avonex	2 (9)	9 (16)	
Betaferon	4 (18)	11 (20)	
Magnetic resonance imaging changes			
New T2-hyperintense lesions	9 (41)	13 (23)	0.06
Contrast-enhancing lesions	7 (32)	11 (20)	0.14
Clinical relapse after interferon use (any)	12 (55)	18 (32)	0.08
No. of clinical relapse after interferon use	1.9±3.2	0.6±1.1	0.01
Clinical status			0.029
Doing well	10 (46)	38 (68)	
Intermediate disease activity	2 (9)	7 (13)	
Doing poorly	10 (46)	11 (20)	

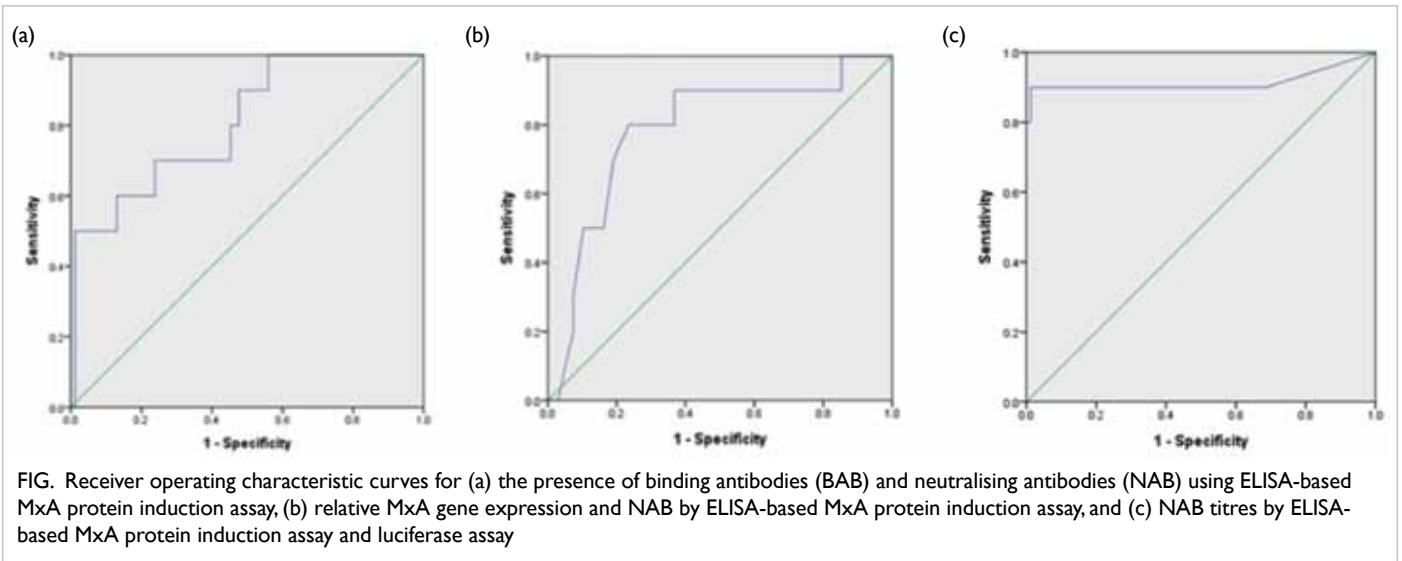


FIG. Receiver operating characteristic curves for (a) the presence of binding antibodies (BAB) and neutralising antibodies (NAB) using ELISA-based MxA protein induction assay, (b) relative MxA gene expression and NAB by ELISA-based MxA protein induction assay, and (c) NAB titres by ELISA-based MxA protein induction assay and luciferase assay

TRU/mL) and 100% concordant results with high titre (100 TRU/mL) cut-off. These results confirmed the reliability of MxA protein induction assay as a confirmatory test for NAB.

Discussion

We evaluated the performance, convenience, and reproducibility of assays for BAB and NAB to IFN-beta in a cohort of 78 Chinese patients with MS.

BAB was present in 78% patients and NAB was found in 28% patients. Patients with high titres of NAB were six times more likely to have poor clinical outcome. This is the first study to determine the prevalence of NAB to IFN-beta in Chinese patients, and substantiate the need for routine clinical testing of NAB in patients treated with IFN-beta.

The prevalence of both BAB (78%) and NABs (28%) were comparable to those reported elsewhere. There were differences between NAB-

positive and NAB-negative patients in terms of clinical and MRI outcomes, especially in patients with high titres of NAB. This is consistent with the proposed detrimental effects of NABs on treatment efficacy, and thus a recommendation to switch therapy should be made. The subcutaneous preparations of IFN-beta had higher proportion (27%-31%) than intramuscular preparation (18%) although did not reach significance. High titres of NAB or very low levels of MxA relative gene expression are strongly associated with presence of NAB.³ The immunological-clinical correlation is less pronounced for patients with low titres of NAB (20-100 TRU/mL). However, this cross-sectional study was unable to evaluate the changes of NABs over time, as low-titre NABs may disappear over time. Nevertheless, it is important to monitor the presence of NAB in patients with MS receiving IFN-beta, as presence of NAB strongly increases the risk of poor clinical response, and recommendation to switch therapy should be considered.

Conclusions

NABs are found in Chinese patients with MS and are associated with poor clinical outcome. MxA relative gene expression and protein induction assays are reliable and complimentary assays to test for NABs.

Routine testing for NABs should be implemented to identify poor responders early in Chinese patients with MS using IFN-beta. The results can be used to develop cost-effective treatment algorithms to identify appropriate patients with MS for second-line therapies.

Acknowledgements

This study was supported by the Health and Medical Research Fund, Food and Health Bureau, Hong Kong SAR Government (#01120486). We thank the neurologists and immunologists from different hospitals in Hong Kong for helping to complete this study. We also thank our research assistants, research nurses, technicians, and many others.

References

1. Compston A, Coles A. Multiple sclerosis. *Lancet* 2008;372:1502-17.
2. Polman CH, Bertolotto A, Deisenhammer F, et al. Recommendations for clinical use of data on neutralising antibodies to interferon-beta therapy in multiple sclerosis. *Lancet Neurol* 2010;9:740-50.
3. Hegen H, Millonig A, Bertolotto A, et al. Early detection of neutralizing antibodies to interferon-beta in multiple sclerosis patients: binding antibodies predict neutralizing antibody development. *Mult Scler* 2014;20:577-87.

Novel beta-amyloid aggregate inhibitors for Alzheimer's disease

RMS Wong *, HW Li, DWJ Kwong, KKL Yung, Y Ke

KEY MESSAGES

1. Carbazole-based cyanines offer neuroprotection against amyloid- β -induced toxicity; thus, they have a potential role in the treatment of Alzheimer's disease.
2. We designed, synthesised, and screened more than 30 carbazole-based cyanines for effective and potent amyloid- β peptide oligomerisation and aggregation inhibitors.
3. Of these, six carbazole-based cyanines that were non-toxic, brain penetrable, and neuroprotective against amyloid- β -induced toxicity were identified as potential candidates for further clinical development.
4. Mice treated with one neuroprotective carbazole-

based cyanine, SLM, showed improvement in cognitive functions, decrease in oligomeric amyloid- β contents and t-tau and p-tau proteins, particularly in the cerebral hippocampal region.

Hong Kong Med J 2019;25(Suppl 5):S26-9

HMRF project number: 01122066

¹ RMS Wong, ¹ HW Li, ¹ DWJ Kwong, ² KKL Yung, ³ Y Ke

¹ Department of Chemistry, Hong Kong Baptist University

² Department of Biology, Hong Kong Baptist University

³ School of Biomedical Sciences, The Chinese University of Hong Kong

* Principal applicant and corresponding author: mswong@hkbu.edu.hk

Introduction

Alzheimer's disease (AD) is the most common form of dementia among older people and causes impairment of many cognitive functions such as memory, thinking, and recognition. More than 47 million people worldwide have AD according to the Alzheimer's Disease International. AD poses tremendous burdens on health care costs and social problems. Although some current AD treatments can improve symptoms, none can stop or reverse its progression. Several approaches that aim to inhibit AD progression have advanced to clinical trials. The most intensely investigated strategies are those targeting the production and clearance of the amyloid- β (A β) peptide, which is closely related to its pathogenesis.

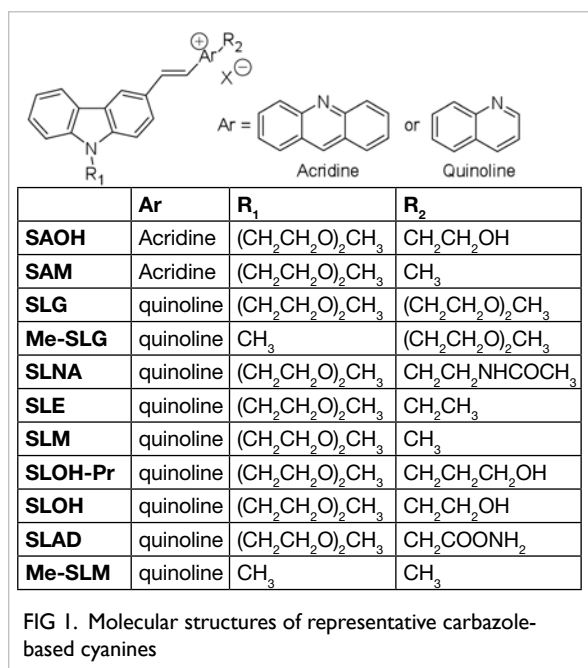
One of the pathological hallmarks of AD is the accumulation of amyloid plaques in the brain. A β peptides, made up of 40 or 42 amino acids, are the major components of the A β plaques found in the brains of AD patients. A β peptides play a central role in the disease process, and their aggregates exert cytotoxic effect towards the neurons and initiate the pathogenic cascade, ie, the amyloid cascade hypothesis.¹ Oligomeric, prefibrillar, and diffusible assemblies of A β peptides are more neurotoxic.² Although there is no consensus on the mechanism for the pathogenic oligomeric assembly, finding brain-penetrating small molecules that can interfere the self-aggregation of A β monomers and thus inhibit the formation of the neurotoxic oligomers and the resulting A β plaques is an attractive approach to

preventing/treating the disease.

In this study, we designed and synthesised a series of novel carbazole-based cyanines to investigate the structure-biological activity properties of these compounds (including bio-availability, blood-brain permeability, neuroprotection against A β -induced toxicity, and *in vivo* efficacy) via cell-based and animal model studies in the roles of AD treatment.

Results and discussion

More than 30 carbazole-based cyanines were designed, synthesised, and screened for effective and potent A β peptide oligomerisation and aggregation inhibitors as neuroprotective and therapeutic agents for AD treatment. Synthesis of the carbazole-based cyanines was carried out by the Knoevenagel reaction or the Wadsworth-Emmons reaction as the key step.³ Some of the representative molecules are summarised in Fig 1. The screening of the potential A β aggregation inhibitors was performed by direct monitoring of the population and length of the resultant fibrils with total internal reflection fluorescence microscopy as well as SDS-PAGE coupled with the photoinduced crosslinking of unmodified proteins protocol. A general correlation between the binding affinity and the inhibitory potency was demonstrated. Acridinium-based cyanines were found to exhibit a stronger binding association with A β ₍₁₋₄₀₎ fibrils (eg, K_d for SAM and SAOH were 11 and 2 μ M, respectively), which also accounted for the pronounced and complete

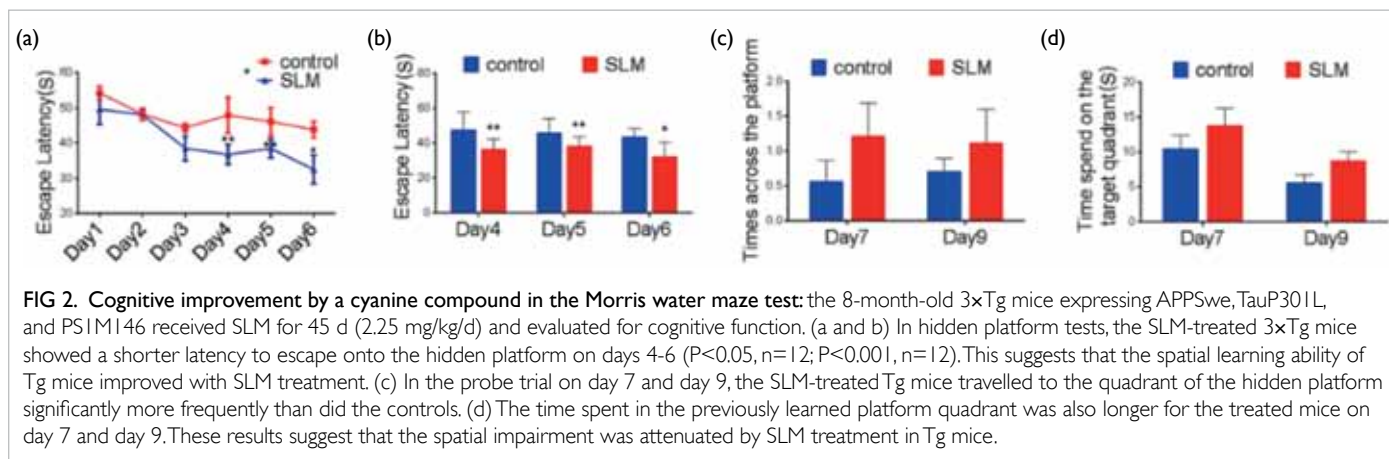


inhibition on the elongation of the Aβ₍₁₋₄₀₎ fibrils. This supported the important role of the hydrophobic and π-π stacking interactions being vital to this type of an association and inhibitory effect. The inhibitory mechanism was investigated by circular dichroism. Upon mixing of monomeric Aβ₍₁₋₄₀₎ with the cyanines, a substantial red spectral shift in the circular dichroism spectra was observed. Such shift indicated the conformational transition of the monomer in the presence cyanine and the formation of the cyanine-Aβ assembly. Hence, an addition of a cyanine to the Aβ peptide monomer could prevent its transition to the amyloidogenic β-sheet-rich conformer, thereby inhibiting its self-aggregation. So far, 18 newly synthesised cyanines have shown effective inhibitory effect on Aβ peptide aggregation.

The cytotoxicities of the new cyanines were

evaluated by the MTT assay on human neuroblastoma (SH-SY5Y) cells at different concentrations (10 nM to 50 μM). Generally, the neuronal cells were highly susceptible to the minor change in the chemical structures of these compounds. The LC₅₀ of some of the inhibitors were determined in the range of 2-133 μM. This confirmed that these inhibitors exhibited low cytotoxicity to neuronal cells. The neuroprotection effect of these non-toxic cyanines against Aβ₍₁₋₄₀₎- and Aβ₍₁₋₄₂₎-induced toxicity was also examined on SH-SY5Y and primary neuronal cells. Only SLE, SLM, SLOH, SLOH-Pr, SLAD, and Me-SLM showed significant neuroprotection in both types of cells, highlighting a potential for further development as neuroprotective and therapeutic agents for AD.

Reactive oxygen species (ROS) have been implicated in premature neuronal cell death in many neurodegenerative diseases. The ability of the inhibitors to reduce Aβ-induced ROS and oxidative stress in neurons was investigated. The ROS level induced by the presence of Aβ₍₁₋₄₀₎ or Aβ₍₁₋₄₂₎ in SH-SY5Y, primary cortical, and hippocampal cells was evaluated by the dichlorofluorescein assay. The results showed that the neuroprotective cyanine inhibitors could reduce the ROS-mediated toxicity induced by Aβ species. It is known that the neurotoxic Aβ oligomers can cause overloading of intracellular [Ca²⁺] leading to cell death. To explore the influence of the cyanines on the Aβ₍₁₋₄₂₎-induced calcium influx, the change in the calcium concentration in the primary hippocampal cells by an addition of Aβ₍₁₋₄₂₎ was monitored by fluo-4 AM indicator under confocal laser scanning microscopy. The results revealed that upon an addition of Aβ₍₁₋₄₂₎, a significant upregulation of [Ca²⁺] occurred. For primary cells pretreated with the selected cyanines, the uploading of [Ca²⁺] induced by Aβ₍₁₋₄₂₎ was readily suppressed. These demonstrated that these cyanines could protect the neuronal cells against Aβ-induced intracellular [Ca²⁺] influx.



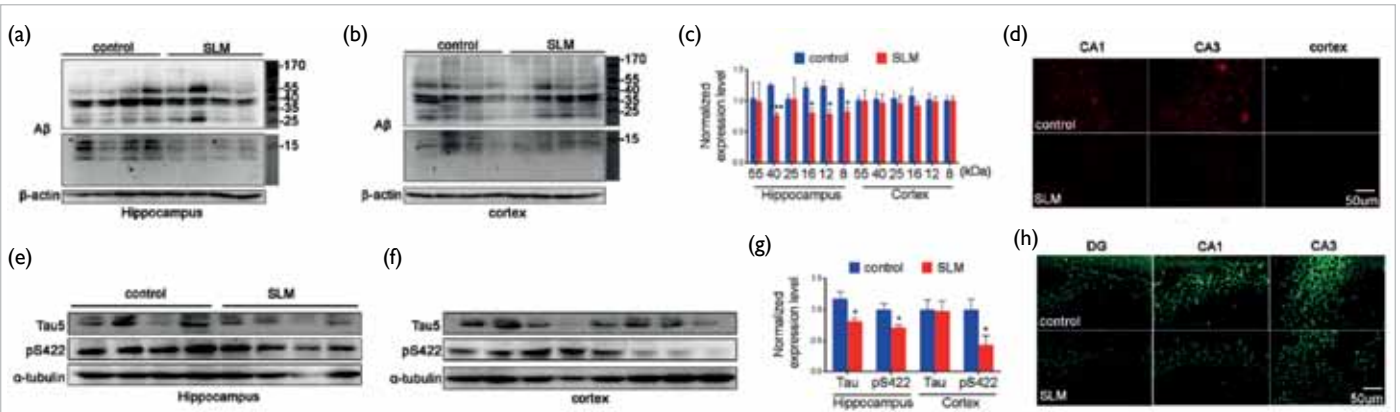


FIG 3. Levels of A β and tau in the hippocampal and cortical region of SLM-treated 3 \times Tg mice were analysed with the western blot and immunofluorescence. The mice were sacrificed, (a to c and e to g) The protein contents of the brain lysates were analysed with the western blot. (d) Brain slices of the hippocampus and the cortex were immunostained using mouse polyclonal antibodies against A β ₍₁₋₄₂₎ followed by Alexa Fluor 488-conjugated Fab fragments of goat anti-mouse immunoglobulin. (h) For tau-5 immunofluorescent staining, the brain slices were labelled with a primary antibody specific for Tau5 followed by Alexa Fluor 488-conjugated Fab fragments of goat anti-mouse immunoglobulin. A β and tau clearly deposited in the cortex and hippocampus of the non-treated Tg mice, whereas the loading of this deposition was significantly reduced upon SLM-treatment, as demonstrated in the brain slices of the treated Tg mice, which correlated with the results of the western blot.

The blood-brain barrier permeability of these A β aggregate inhibitors is important for potential *in vivo* applications. Therefore, the tail-vein injection of the cyanine into normal and transgenic mice was conducted. These cyanines generally exhibited a strong fluorescence signal in the wavelength range of 600-650 nm in brain tissues; therefore, the blood-brain barrier permeability was readily confirmed by the confocal fluorescence images of the cyanine signals. Encouragingly, all the newly developed neuroprotective cyanine inhibitors were found to be blood-brain barrier penetrable.

In addition, the LD₅₀ were determined to be in the range of 47 to >125 mg/kg in order to provide a safe dosage of these cyanines for test animals. These findings consistently confirmed that these cyanines are of low acute toxicity in the test animals.

To explore the potential of a neuroprotective cyanine, SLM, on halting or slowing the cognitive impairment, we conducted an animal model study on APP^{swE}/TauP301L/PS1M146 transgenic mice. As these 3 \times Tg-AD mice showed intracellular A β in 3- to 6-month-old mice and cognitive impairment in 6-month-old mice, the 8-month-old 3 \times Tg-AD mice were treated with SLM for 45 days (2.25 mg/kg/d) intraperitoneally. After the 45-day SLM-treatment, the Morris water maze test was performed. The control group of 3 \times Tg-AD mice was included in the test for comparison. The treated and non-treated 3 \times Tg-AD mice were trained for 1 day (4 trials per day). Initially, the two groups showed similar escape latency and similar swimming speed on the first training day, indicating that SLM produced no effect on the vision and motility of the 3 \times Tg-AD mice. After the vision platform training, the mice were

introduced to hidden platform tests for 5 days. In hidden platform tests, the SLM-treated 3 \times Tg-AD mice exhibited a significantly shorter latency to escape onto the hidden platform during days 4 to 6 than did those of the control group on days 1 to 6 (Fig 2). Furthermore, a probe trial was performed to assess the memory retention of the mice on day 7 and day 9. The SLM-treated 3 \times Tg mice travelled to the previously learned platform quadrant more frequently than the control ones. The time spent in the previously learned platform quadrant was also longer for the treated 3 \times Tg mice on day 7 and day 9. These results consistently indicated that the SLM-treated 3 \times Tg mice showed a significant cognitive improvement after 45 days of treatment, not only enhancing learning skills in the hidden platform test but also improving the spatial memory in the probe trial.

To determine the effect of SLM on A β and tau pathologies in 3 \times Tg AD mice after behavioural testing, the deposition of the A β and tau contents in the brain of the SLM-treated Tg mice were determined via multiple biochemical analyses, including the western blot analysis and immunofluorescence. Remarkably, the A β content substantially decreased, in particular those of toxic A β oligomers with MW of 8, 12, 16, 25, 40, and 55 kD, as did the total tau (tau-5) and phosphorylated-tau (ps422) proteins in hippocampal regions, as compared with those of the controls (Fig 3), suggesting that the cyanine inhibitor can ameliorate both A β and tau pathologies in the 3 \times Tg-AD mouse model. The size of neuritic plaques and the amount of A β and tau content were lower than those of the control 3 \times Tg-AD mice (Fig 3) as visualised by immunostaining in brain slices. In

addition, the level of inactive glycogen synthase kinase-3 β (GSK3 β) was significantly higher in the SLM-treated Tg mice, likely explaining for the decrease in the phosphorylated tau content.

Increasing evidence implicates that autophagy plays a crucial role in the pathogenesis of AD. Thus, we investigated whether SLM treatment would modulate autophagic pathway by western blot of Tg mouse brains after the aforementioned behavioural studies. It was found that SLM treatment significantly reduced the level of a key gatekeeper of autophagy, mammalian target of rapamycin (mTOR), which was down-regulated by the substantial decrease in an upstream effector, Akt and an increase in the proautophagic protein, mammalian orthologue of yeast Atg6 (Beclin 1) level. In addition, there was a marked reduction in microtubule-associated protein light chain 3-II (LC3-II) level and the LC3-associated protein p62 (sequestosome 1), a marker of autophagic flux also showed a decreasing trend. Meanwhile, the level of the lysosomal protease Cathepsin D (CatD) that mediates the degradation in autophagolysosomes was significantly increased. All these results consistently support that autophagic flux is induced in 3 \times Tg-AD mice upon SLM treatment resulting in the reduction in amyloid deposits and tau contents as well as improvement of cognitive deficits in the AD mouse model.

Conclusions

The present study represents the first *in vivo* evidence

that the carbazole-based cyanines can ameliorate both A β and tau pathologies together with reduction in the levels of toxic A β oligomers and p-tau protein, representing an important advancement in AD drug development.

Acknowledgements

This work was supported by the Health and Medical Research Fund, Food and Health Bureau, Hong Kong SAR Government (#01122066) and Interdisciplinary Research Matching Scheme of Hong Kong Baptist University (RC-IRMS/12-13/01). We thank the support of the National Natural Sciences Foundation of China (No. 81400847), the Young Scientists Fund from the National Science Foundation of China (21205006), and the University Grants Council, Hong Kong SAR (GRF/HKBU201612). The Institute of Molecular Functional Materials was supported by a grant from the University Grants Committee, Hong Kong, Areas of Excellence Scheme (AoE/P-03/08).

References

1. Makin OS, Serpell LC. Structures for amyloid fibrils. *FEBS J* 2005;272:5950-61.
2. Cohen FE, Kelly JW. Therapeutic approaches to protein-misfolding diseases. *Nature* 2003;426:905-9.
3. Yang W, Wong Y, Ng OT, et al. Inhibition of beta-amyloid peptide aggregation by multifunctional carbazole-based fluorophores. *Angew Chem Int Ed Engl* 2012;51:1804-10.

Prenatal diagnosis of pathogenic genomic imbalance in fetuses with increased nuchal translucency but normal karyotyping using chromosomal microarray

TY Leung *, KC Au Yeung, WC Leung, KY Leung, TK Lo, WWK To, WL Lau, LW Chan, DS Sahota, RKW Choy

KEY MESSAGES

1. 3.7% of fetuses with increased nuchal translucency (≥ 3.5 mm) but normal karyotype had pathogenic genomic imbalance.
2. The incidence of pathogenic copy number variants was higher among fetuses with increased nuchal translucency in terms of sonographic anomalies (9.7%), compared with those without (3.0%).
3. Fetuses with increased nuchal translucency (≥ 3.5 mm) should be considered further testing with chromosomal microarray.

Hong Kong Med J 2019;25(Suppl 5):S30-2

HMRP project number: 01120766

¹ TY Leung, ² KC Au Yeung, ³ WC Leung, ⁴ KY Leung, ⁵ TK Lo, ⁶ WWK To, ³ WL Lau, ⁶ LW Chan, ¹ DS Sahota, ¹ RKW Choy

¹ Department of Obstetrics & Gynaecology, The Chinese University of Hong Kong

² Department of Obstetrics & Gynaecology, Tuen Mun Hospital

³ Department of Obstetrics & Gynaecology, Kwong Wah Hospital

⁴ Department of Obstetrics & Gynaecology, Queen Elizabeth Hospital

⁵ Department of Obstetrics & Gynaecology, Princess Margaret Hospital

⁶ Department of Obstetrics & Gynaecology, United Christian Hospital

* Principal applicant and corresponding author: tyleung@cuhk.edu.hk

Introduction

In 2010, Hong Kong launched universal first trimester Down syndrome screening using fetal nuchal translucency (NT) and biochemical assay. For screened positive cases, fetal karyotyping by chorionic villus sampling or amniocentesis is recommended. This screening strategy has achieved a high detection of 90%, with a false positive rate of 5%.¹ Although normal fetal karyotyping may be reassuring, these screened positive fetuses, especially if the NT is markedly increased (>95th centile), are at higher risk of developing structural abnormalities and neurodevelopmental delay during childhood. These structural and neurodevelopmental abnormalities may be associated with a wide variety of genetic or genomic diseases that may not be revealed by conventional chromosome analysis.

Prenatal diagnosis for these genetic or genomic diseases is difficult, because some diseases may be associated with morphological abnormalities that are very subtle and non-specific on ultrasonography, and appear in the later gestation or even postnatally. In addition, although over 100 diseases have been reported to be associated with an increased NT, such association has not been fully explored, and more diseases are expected to be discovered in future. Therefore, a more comprehensive genetic test is required to diagnose or exclude these genetic or genomic diseases prenatally.

Chromosomal microarray (CMA) can detect genomic imbalance (microdeletion / microduplication) and offer >40 times the resolution of karyotyping. CMA has dramatically improved the reliability of detecting copy number variants (CNVs) and subtle chromosomal abnormalities, including many disorders not detectable by an optimal karyotype, FISH or DNA direct sequencing. Our preliminary retrospective study has shown that pathogenic genomic imbalance occurred in 4 out of 48 stored DNA samples (8.3%) from fetuses with normal karyotyping but increased NT (≥ 3.5 mm; 99th centile). A prospective study with larger sample size is required to estimate the prevalence of pathogenic genomic imbalance among this group of patients.

Methods

This was a prospective study by six obstetric units (Kwong Wah Hospital, Prince of Wales Hospital, Princess Margaret Hospital, Queen Elizabeth Hospital, Tuen Mun Hospital, and United Christian Hospital). Women who presented to these units for first trimester combined screening test and had fetal NT ≥ 3.5 mm despite normal karyotyping (either via chorionic villus sampling or amniocentesis) were invited to participate. Fetal samples were further examined for any genomic CNVs using a custom-designed high-resolution 44K oligonucleotide array.

Parental bloods were also sampled to determine if the fetal CNVs was inherited. Samples were analysed in prenatal diagnostic laboratory, Department of Obstetrics and Gynaecology, The Chinese University of Hong Kong. Chromosomal microarray was analysed via CytoGenomics (Agilent Technologies). Chromosomal structural variant detection was based on our reported method.²⁻⁴ Pathogenic CNVs or variants of uncertain significance (VOUS) were classified in accordance to the American College of Medical Genetics and Genomics guidelines using chromosomal microarray-based databases (ClinVarCNV, DECIPHER) and internal databases from The Chinese University of Hong Kong. Patients detected with pathogenic CNVs and VOUS were contacted for further counselling.

Results

A total of 300 fetuses with NT ≥ 3.5 mm and normal karyotyping were recruited. Samples included 252 chorionic villus samples, 44 amniotic fluid, and 4 fetal tissue samples (after termination of pregnancy). The NT measurement ranged from 3.5 mm to 14 mm, with a median of 4.3 mm. 31 (10.3%) cases were detected to have additional structure abnormalities by ultrasound in the first trimester (syndromic), whereas the rest (89.7%) only had isolated high NT. The risk of syndromic malformation increased with NT thickness; it was 4% when NT was 3.5-4 mm, 8.6% when 4-5.5 mm, and 25.4% when ≥ 5.5 mm.

Eleven cases (3.7%) were identified to have pathogenic CNVs. The incidence of pathogenic CNVs in the syndromic group (3/31, 9.7%) was higher than the isolated group (8/269, 3.0%) but not statistically significantly ($P=0.09$, Fisher's exact test). The prevalence of pathogenic CNVs was 3.7%, 4.5%, and 5.1% when the NT thickness was ≥ 3.5 mm, ≥ 4.0 mm, and ≥ 5.5 mm, respectively. The size of genomic imbalance ranged from 14 kb to 10 Mb. Three cases (27.3%) were detected with two CNVs indicating that complex genomic rearrangement may be the underlying cause for increased NT and other abnormalities. In these 11 cases, one chose to keep pregnancy to live birth, nine chose termination of pregnancy, and one lost to follow-up.

In 14 (4.7%) cases, their CNVs were classified as VOUS, which were about 0.3 Mb to 7 Mb in size. None was detected to have any other fetal structural abnormalities. Twelve cases were live births and two cases lost to follow-up.

Six cases had uncertain significance after karyotyping and required CMA to determine pathogenicity. Three of them were confirmed to be pathogenic. The first case was a 47XY, +mar with a 10 Mb triplication on 15q11.1q13.2, which contained the Prader-Willi/Angelman critical region. After counselling the patient chose medical termination of pregnancy. The abortus did not show

any obvious structural abnormality (consistent with ultrasound findings). The second case was 46,XX,del(8)(p23.1) of 6 Mb. The karyotype analysis on this was not confident due to the relative low resolution around 5-10 Mb. CMA helped confirm the karyotype abnormal findings. The third case was 46,XY,add(9)(?:p?22)->qter)dn, which turned out to be an 18 Mb deletion on chromosome 9p22.2-24.2. The other three cases had normal CMA results and were regarded as normal variants (46, XX, 22p-, 46,XY,9p+, 47XY, +mar) inherited from the parents and proceeded to livebirths.

Discussion

In this study, 3.7% of fetuses with significantly increased NT (≥ 3.5 mm; 99th centile) but normal karyotypes were found to have pathogenic genomic imbalance through CMA. This incidence was lower than the 8% in our retrospective study of 40 cases collected from Denmark,⁵ but was higher than the 1.4% in our retrospective study of 215 samples collected from the United Kingdom.⁶ The Chinese cohort in this study was most representative to our local population.

Our finding was comparable to that reported in a systematic review in 2015.⁷ It found that the incidence of pathogenic CNV was 4% (54/1403) in cases with only isolated thick NT and 7% (20/251) when associated with other fetal structural abnormalities. In our cohort, the pathogenic CNV rate of 9.7% in the syndromic NT group was higher than that in the isolated NT group (3.0%) although the difference did not reach statistical significance. Thus, CMA may be indicated in the former group but not the latter group, as recommended by the American College of Obstetricians and Gynecologists.⁸

Whether CMA is indicated in cases with isolated thick NT is debatable. First, 3% to 4% (1/33-1/25) chance of pathogenicity is not low, especially if termination of pregnancy is considered. Second, during the first trimester the fetus is too small to confirm or exclude any fetal malformations and to determine whether it is syndromic or simply isolated thick NT (as shown in our two cases). Hence, a follow-up morphology scan in the second trimester is essential. However, the drawback is that affected parents may have to wait for weeks and this may create anxiety. Furthermore, if abnormal CMA result can be known earlier, first trimester termination of pregnancy is preferred to second trimester in term of maternal physical and psychological health. Third, cystic hygroma is traditionally regarded as a 'soft marker' and not a 'structural' malformation, and hence was not categorised to the syndromic group. However, cystic hygroma is commonly associated with syndromic disorders and should be taken seriously. After considering the potential benefits of early CMA and limitation of ultrasonography,

it is worthwhile to perform CMA for cases with apparently isolated thick NT.

Six cases with karyotyping showing uncertain significant results were not included in our study. Their karyotypes could not be classified as normal or abnormal because of the presence of marker chromosomes or because of the limited banding. However, such conditions are not uncommon in our daily practice (2% in our cohort), and thus CMA has a role in delineating pathogenicity and assisting in clinical management.

In our cohort, the VOUS rate of 4.7% was higher than the generally cited rate of 1% to 3%. One reason may be ethnic group differences. With proper consulting, all VOUS cases kept pregnancy. Twelve of these 14 cases had live birth and were followed up to 6 months old without obvious developmental problem. Long-term follow-up is needed to ensure the developmental outcomes of these babies.

Conclusions

Our study indicated that 3.7% of fetuses with significantly increased NT (>3.5 mm) despite normal karyotype had pathogenic genomic imbalance detected by CMA. The incidence was higher in the syndromic group (9.7%) than the isolated NT group (3.0%). Hence, CMA is warranted to search for any pathogenic CNVs after karyotyping has excluded common chromosomal abnormalities.

Acknowledgements

This study was supported by the Health and Medical Research Fund, Food and Health Bureau, Hong Kong SAR Government (#01120766). We thank the clinical colleagues from all study centres who supported subject recruitment and the laboratory colleagues

at the Prince of Wales Hospital and The Chinese University of Hong Kong for their help in facilitating this study. We would also like to acknowledge all research participants for contribution of samples.

References

1. Sahota DS, Leung WC, Chan WP, To WW, Lau ET, Leung TY. Prospective assessment of the Hong Kong Hospital Authority universal Down syndrome screening programme. *Hong Kong Med J* 2013;19:101-8.
2. Cao Y, Li Z, Rosenfeld JA, et al. Contribution of genomic copy-number variations in prenatal oral clefts: a multicenter cohort study. *Genet Med* 2016;18:1052-5.
3. Huang J, Poon LC, Akolekar R, Choy KW, Leung TY, Nicolaides KH. Is high fetal nuchal translucency associated with submicroscopic chromosomal abnormalities on array CGH? *Ultrasound Obstet Gynecol* 2014;43:620-4.
4. Leung TY, Vogel I, Lau TK, et al. Identification of submicroscopic chromosomal aberrations in fetuses with increased nuchal translucency and an apparently normal karyotype. *Ultrasound Obstet Gynecol* 2011;38:314-9.
5. Cheng YK, Huang J, Law KM, Chan YM, Leung TY, Choy KW. Prenatal diagnosis of maternally inherited X-linked Opitz G/BBB syndrome by chromosomal microarray in a fetus with complex congenital heart disease. *Clin Chim Acta* 2014;436:140-2.
6. Huang J, Poon LC, Akolekar R, Choy KW, Leung TY, Nicolaides KH. Is high fetal nuchal translucency associated with submicroscopic chromosomal abnormalities by array CGH? *Ultrasound Obstet Gynecol* 2014;43:620-4.
7. Grande M, Jansen FA, Blumenfeld YJ, et al. Genomic microarray in fetuses with increased nuchal translucency and normal karyotype: a systematic review and meta-analysis. *Ultrasound Obstet Gynecol* 2015;46:650-8.
8. American College of Obstetricians and Gynecologists' Committee on Practice Bulletins—Obstetrics; Committee on Genetics; Society for Maternal–Fetal Medicine. Practice Bulletin No. 162: Prenatal diagnostic testing for genetic disorders. *Obstet Gynecol* 2016;127:e108-22.

Placental biology of Down syndrome in relation to increased gene dosage

OGW Wong, HYS Ngan, ANY Cheung *

KEY MESSAGES

1. Amyloid precursor protein (APP) is overexpressed in the placentas of Down syndrome subjects.
2. Inducible APP overexpressed trophoblast cell line models are established.
3. APP overexpression dysregulates trophoblast cell functions.

Hong Kong Med J 2019;25(Suppl 5):S33-5

HMRF project number: 01120936

¹ OGW Wong, ² HYS Ngan, ¹ ANY Cheung

Queen Mary Hospital, The University of Hong Kong:

¹ Department of Pathology

² Department of Obstetrics and Gynaecology

* Principal applicant and corresponding author: anycheun@pathology.hku.hk

Introduction

Down syndrome (DS) is the most common congenital abnormality in humans. Trisomy 21 is the major cause and accounts for about 95% of DS. DS manifests a spectrum of phenotypes, including retardation in cognitive ability and physical growth, cardiac defects, craniofacial alterations, and muscle hypotonia.¹ Among women diagnosed to have DS fetus by prenatal screening, the induced abortion rate is estimated to be 50% to 90%. A reduction in the termination rate is observed in recent years, and hence there may be an increasing number of DS individuals whose medical conditions need to be taken care of. Functional characterisation of genes dysregulated in DS may facilitate development of potential gene therapy strategies to correct phenotypic abnormalities in DS.

Defects in DS placentas have been well documented.² Histologically, more conspicuous two-layered trophoblast in the chorionic villi of trisomy 21 placentas is noted secondary to increased presence of mononuclear cytotrophoblast. Cultured villous cytotrophoblast cells from trisomy 21 aggregate normally but fuse inefficiently to form multinucleated syncytiotrophoblast. DS placenta also exhibits dysregulated hCG physiology. The number of mature hCG receptor (LH/CG-R) molecules expressed on the surface of trisomy 21-affected cytotrophoblasts is significantly reduced. Nonetheless, the molecular basis underlying the alteration in trophoblast differentiation and hCG signalling in DS trisomy 21 placentas are largely unknown.

Various genetic mechanisms of DS have been suggested. For instance, critical regions in chromosome 21 may account for pathogenesis of DS. Various phenotypes of DS are considered to be results of the extra copy of dosage sensitive genes among the genes present on human chromosome 21

(the 'gene dosage' hypothesis). A list of genes with direct evidence of increased dose or allelic variation that may induce one or more phenotypes of DS has been compiled.³ Placental dysfunction is associated with intrauterine growth retardation, hypertension, hypoxic-ischaemic injury, preterm labour, and fetal death. Trophoblast cell biology plays important roles in these diseases. For example, aberrant cell death signals are associated with increased p53 activity and altered translation of AKT, and mTOR proteins are crucial in pathogenesis of intrauterine growth retardation.⁴ Moreover, almost all DS individuals suffered from stunted growth at birth and in adulthood. Therefore, it is important to include a placental trophoblast model in the study of DS.

This study aimed to (1) investigate the expression profiles of amyloid precursor protein (*APP*), *ETS2*, *SOD1*, and *HMGNI*, in trisomy 21 placentas, (2) establish inducible overexpression trophoblast cell line models, (3) investigate the phenotypic (proliferation, apoptosis, invasion, hCG secretion, LH/CG-R expression, and differentiation) changes of trophoblast upon overexpression of dosage sensitive genes, and (4) delineate the molecular mechanisms of dosage sensitive genes with particular focus on the hCG-PI3K-Pak4 and Nanog signalling pathways known to affect trophoblast pathology.

Methods

A total of 71 formalin-fixed paraffin-embedded placental tissues, including 37 placentas from normal pregnancies and 34 placentas from DS pregnancies were retrieved from the archive of Department of Pathology, Queen Mary Hospital. The use of the samples was approved by the institutional review board of the University of Hong Kong/Hospital Authority Hong Kong West Cluster (ref. UW 13-124).

Five 10- μ m sections were cut from each placenta and the total RNA was extracted using the RNeasy FFPE kit (Qiagen). At least 500 ng total RNA was reverse-transcribed into cDNA using the PrimeScript RT kit (Clontech). Each RT-qPCR reaction contains 1X HotStart SYBR Green qPCR master mix (Excell), 1 μ M forward primer, 1 μ M reverse primer, 0.5 μ L cDNA, and 4.5 μ L milli-Q water. RT-qPCR reactions were run using the 7900HT Fast Real-Time PCR System (Applied Biosystems).

Immunohistochemical study was performed with antigen retrieval through heating under pressure. The sections were then incubated with anti-APP antibody (ab32136, Abcam) at room temperature overnight and the signal was visualised using the EnVision+ Dual Link System. The stained sections were scanned with the Aperio slide scanner, and the staining intensity was evaluated by the positive pixel count v9 algorithm provided by the system.

Western blot was performed according to standard procedures. Antibodies used included: APP (ab32136, Abcam), GFP (ZsGreen, 632598, clontech), β -actin (A5060, Sigma-Aldrich), Caspase 3 (#9662, Cell Signaling), LHCGR (19968-1-AP, Proteintech), PAK4 (#3242, Cell Signaling), p-PAK4 (#3241, Cell Signaling), NANOG (14295-1-AP, Proteintech), p-PI3K p85 (#4228, Cell Signaling), PI3K p85 (#4257, Cell Signaling), and Akt (#9272, Cell Signaling).

The functional implication of APP overexpression was investigated in two trophoblast cell line HTR-8/SVneo.⁵ HTR-8/SVneo was stably transfected with a Tet-On expression plasmid pTRE3G-BI-APP and yielded two clones B2 and B10. APP was induced in B2 and B10 by including the recombinant protein Tet-Express (Clontech) in the culture medium.

Cell growth and cell proliferation was measured by the MTT assay and BrdU assay, respectively. Cellular senescence was detected using senescence associated β -gal assay. Cell cycle analysis was performed by flow cytometry. Cell migration and invasion activities were measured by transwell migration/invasion assay.

Results

APP is overexpressed in the placentas of Down syndrome

Four candidate genes: *SOD1*, *ETS2*, *APP*, and *HMGNI* located on chr21 were selected for expression characterisation in DS placentas using RT-qPCR. *YWHAZ*, a gene previously demonstrated to be a good reference gene for gene expression study in placenta,⁶ was used as the reference gene. We observed that APP was significantly overexpressed

in DS than normal placentas (mean, 2.498-fold; $P=0.0009$). In addition, *HMGNI* was markedly suppressed in DS than normal placentas (mean, 0.2714-fold; $P<0.0001$). *ETS2* and *SOD1* did not show obvious change in expression between DS and normal placentas. Two additional reference genes *GAPDH* and *TOPI* were used for calculation and yielded similar observations.

The overexpression of APP in DS placenta was verified by immunohistochemistry. Cytoplasmic immunoreactivity was found with focal membranous accentuation. The immunoreactivity was present at cytotrophoblast, syncytiotrophoblast, extravillous implantation site trophoblast, and villous stromal cells. There was a significant increase in APP protein expression in DS than normal placentas ($P<0.0001$) [Fig].

APP overexpression suppressed growth and invasiveness of trophoblast

Growth curves constructed by the MTT assay suggested that APP induction mildly slowed cell growth. This effect was not due to reduced cell proliferation upon APP overexpression, as BrdU incorporation rate did not show significant difference in cells with or without APP induction. Instead, there was an increase in the number of apoptotic cells as in APP-induced B2 and B10 cells as evidenced by flow cytometry analysis of DNA fragmentation, TUNEL assay, and caspase-3 cleavage assay. B2 and B10 cells migrated and invaded slower through transwells when APP was induced.

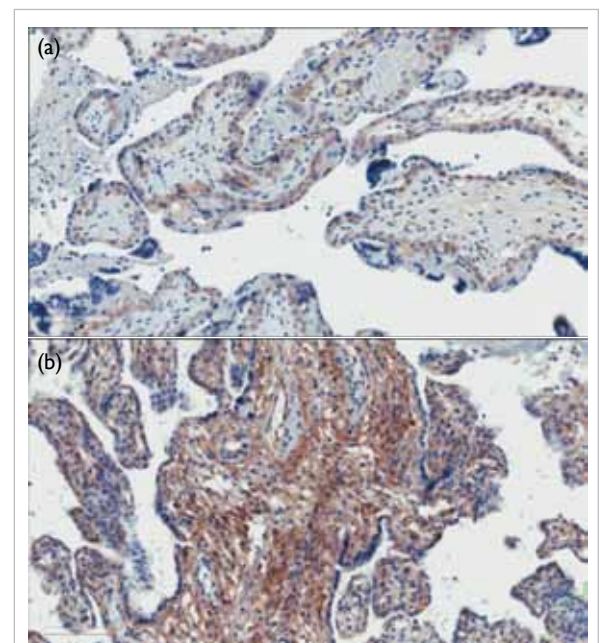


FIG. Cellular expression pattern of amyloid precursor protein in (a) normal and (b) Down syndrome placentas.

APP induction dysregulated hCG level

Reduced alpha and beta hCG mRNA was observed in APP-induced B2 and B10 cells in association with reduced syncytialisation. However, no change in LH/CG-R, PAK4, p-PAK4, or NANOG protein expression could be detected upon APP induction. Expression level and phosphorylation status of PI3K were not affected by APP.

APP was confirmed to be overexpressed in DS placentas in association with dysregulation of trophoblast cell functions. This may contribute to the abnormal phenotypes observed in DS placentas.

Discussion

APP is the very first protein known to be upregulated in the brain of DS individuals.⁷ APP is associated with mental underdevelopment, and DS individuals frequently develop Alzheimer disease at young age. APP is implicated in the abnormalities seen in other organs of DS subjects as well. We confirmed that APP is overexpressed in the placentas of DS subjects. The mRNA expression was accessed by RT-qPCR, and the upregulation was confirmed by immunohistochemistry.

We then investigated the pathological function of APP in DS placentas by establishing inducible expression systems in two trophoblast models HTR-8/SVneo. Doses of inducer APP were manipulated so that the induced protein expression level in HTR-8/SVneo was comparable to what is observed in the clinical samples. APP overexpression in HTR-8/SVneo was found to induce reduction of cell growth in relation to increased apoptosis as evidenced by flow cytometry, TUNEL, and caspase-3 cleavage assays. APP has been shown to participate in apoptosis induction in olfactory neurons.⁸ Cytotrophoblast differentiation into syncytiotrophoblast was suppressed as evidenced by reduced hCG production and syncytialisation. Upon APP induction, reduced trophoblast motility was also observed. Previous characterisation of DS trophoblast has revealed that these cells failed to properly switch their expression of stage-specific antigens towards an invasive phenotype.⁹ Invasive ability of trophoblasts at decidua and maternal blood

vessels play critical role in various functions of the placenta.¹⁰

Conclusion

Dysregulation of trophoblast cell functions upon APP induction may play a role in abnormal placental development in DS individuals.

Acknowledgements

This study was supported by the Health and Medical Research Fund, Food and Health Bureau, Hong Kong SAR Government (#01120936). We thank all patients, doctors, and technical and secretarial colleagues for their assistance in this project.

References

1. Antonarakis SE, Lyle R, Dermitzakis ET, Reymond A, Deutsch S. Chromosome 21 and down syndrome: from genomics to pathophysiology. *Nat Rev Genet* 2004;5:725-38.
2. Pidoux G, Gerbaud P, Cocquebert M, et al. Review: human trophoblast fusion and differentiation: lessons from trisomy 21 placenta. *Placenta* 2012;33(Suppl):S81-6.
3. Lana-Elola E, Watson-Scales SD, Fisher EM, Tybulewicz VL. Down syndrome: searching for the genetic culprits. *Dis Model Mech* 2011;4:586-95.
4. Scifres CM, Nelson DM. Intrauterine growth restriction, human placental development and trophoblast cell death. *J Physiol* 2009;587:3453-8.
5. Graham CH, Hawley TS, Hawley RG, et al. Establishment and characterization of first trimester human trophoblast cells with extended lifespan. *Exp Cell Res* 1993;206:204-11.
6. Meller M, Vadachkoria S, Luthy DA, Williams MA. Evaluation of housekeeping genes in placental comparative expression studies. *Placenta* 2005;26:601-7.
7. Rumble B, Retallack R, Hilbich C, et al. Amyloid A4 protein and its precursor in Down's syndrome and Alzheimer's disease. *N Engl J Med* 1989;320:1446-52.
8. Cheng N, Jiao S, Gumaste A, Bai L, Belluscio L. APP overexpression causes A β -independent neuronal death through intrinsic apoptosis pathway. *eNeuro* 2016;3(4).
9. Wright A, Zhou Y, Weier JE, et al. Trisomy 21 is associated with variable defects in cytotrophoblast differentiation along the invasive pathway. *Am J Med Genet A* 2004;130A:354-64.
10. Knofler M, Pollheimer J. Human placental trophoblast invasion and differentiation: a particular focus on Wnt signaling. *Front Genet* 2013;4:190.

Whole exome sequencing to uncover genetic variants underlying congenital cystic adenomatoid malformations

PK Tam*

KEY MESSAGES

1. Congenital pulmonary airway malformation is a risk factor for paediatric adenocarcinoma of the lungs.
2. Both point mutations in coding sequences and copy number variants involving gene deletions and duplications are recurrently mutated in patients with congenital pulmonary airway malformation but not in the general population.
3. Congenital pulmonary airway malformation is genetically heterogeneous with different mutated genes in different patients. Mutations in more than one gene and/or copy number variants
4. Despite the diversity, mutated genes encode interacting proteins that are members of the same cancer pathway may be a potential therapeutic target.

Hong Kong Med J 2019;25(Suppl 5):S36-8

HMRF project number: 01121576

PK Tam

Department of Surgery, The University of Hong Kong

* Principal applicant and corresponding author: paultam@hku.hk

Introduction

Congenital pulmonary airway malformation (CPAM) is characterised by fetal hamartomatous pulmonary lesions that result from abnormal overgrowth of tracheal, bronchial, bronchiolar, or alveolar tissues. Most CPAMs present antenatally. The clinical presentation ranges from the most serious phenotype that may result in hydrops fetalis and termination of pregnancy to mild phenotype with possible resolution. Affected new-borns present with severe respiratory distress or remain asymptomatic until later in life. Surgical resection is the definitive treatment.¹ Primary adenocarcinomas of the lung in paediatric patients are preponderantly found in conjunction with congenital CPAM and are considered a risk factor for paediatric cancer.²

CPAM is caused by a defective branching morphogenesis of the lung at different developmental stages; however, the trigger for this developmental defect is unknown.¹ Data on the molecular basis underlying CPAM are scant and consist of gene expression analyses in fetal or postnatal resected human CPAM tissues or in animal models. Yet, these studies have identified deregulation of genes/proteins crucial for lung morphogenesis and patterning. Thus, alteration of the signalling pathways controlling lung development is likely the mechanism underlying CPAM. Plausibly, DNA alterations in gene members of the involved pathways could lead to CPAM. The disorder has not been linked to race, maternal age, or exposures.¹

There are gaps in knowledge and uncertainties/controversies in management of CPAM. No genetic study has been conducted on CPAM, likely because

there is no evidence for a classic genetic inheritance of the disorder together with the scarcity of patients. Nonetheless, identical twins affected with CPAM born to unaffected parents have been reported.³ CPAM appears mainly sporadically at a very low incidence (1/8300 and 1/35,000 live births). Thus, we aim to investigate the genetics underlying CPAM under the hypothesis that rare *de novo* or recessive inherited damaging genetic variants in genes governing the development of airways may trigger the disorder and account for the sporadic presentation and scarcity of CPAM.

Results

Sample processing

All patients had a normal karyotype. One trio was excluded owing to an accidental sample duplication. One patient who had bilateral lung hypoplasia was excluded because it might suggest different disease aetiology. Therefore, 18 trios were analysed.

De novo exonic variants

We identified 13 non-synonymous novel *de novo* damaging variants in 13 genes distributed among 11 patients. We then queried Clin Var, Online Mendelian Inheritance in Man database, COSMIC, and Mouse Genome Informatics database to assess the involvement of CPAM genes carrying those *de novo* mutations in other human disorders. There were 23 rare (MAF, $\leq 0.5\%$) or *de novo* coding DNA sequence mutations in 23 genes. Eight of the 23 genes were involved in human genetic diseases, and a novel protein truncating variant was detected in CEP295

(centrosomal protein 295). In addition, 21 of the 23 genes were involved in either adenocarcinoma or small cell carcinoma. *CACNA1H*, *EPG5*, *TRIP12* have been reported to be >50 times in adenocarcinoma samples in COSMIC database. As to the phenotype caused by these mutated genes in mouse/human orthology with phenotype annotations, 16 of 23 genes have been reported in different developmental phenotypes. CPAM patients with mutations in genes known to be involved in other congenital human disorders were clinically re-assessed, and no other conjunctive congenital human disorders was observed.

Inherited exonic variants: homozygosis, compound heterozygosity and di-genic models

We then assessed patients for inherited damaging variants acting in a recessive manner including homozygous, compound heterozygous, and digenic inheritance mutations. For rare homozygous mutations, we detected 24 mutations in 23 genes. Among 24 homozygous mutations, 20 were predicted to be deleterious by logistic regression in 11 CPAM patients. After assessing the involvement of the CPAM genes carrying rare homozygous mutations in other human disorders, two variants were reported in ClinVar including the homozygous mutations

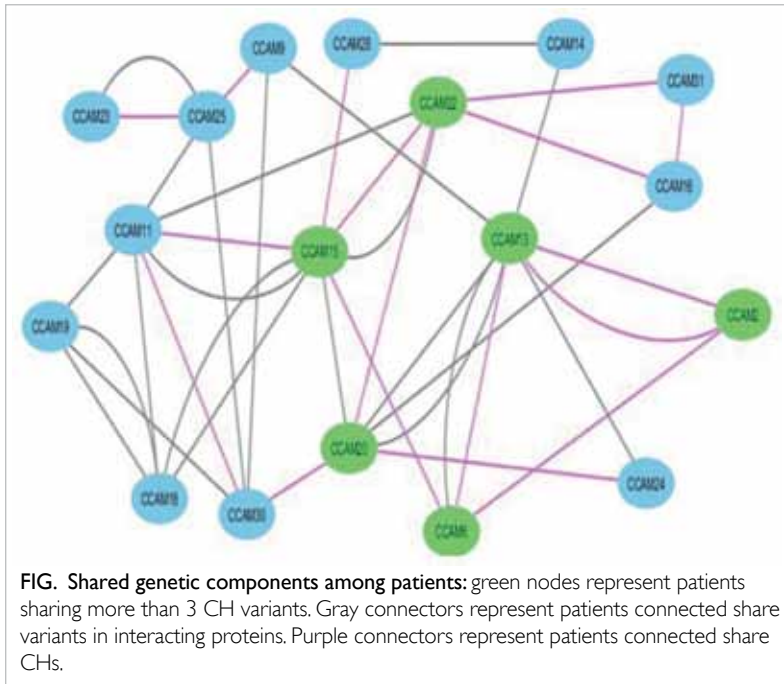
on *LHB* and *PGAM2* genes. Also, 8 of 23 genes were reported in Online Mendelian Inheritance in Man database, and 12 of 23 genes were reported in Mouse Genome Informatics database. All of the rare homozygous mutated genes were involved in adenocarcinoma according to the COSMIC database. Importantly, patient CCAM11C and CCAM22C had identical rare homozygous damaging mutation in *LTBP2* gene. According to ProteomicsDB, *LTBP2* has highest RNA expression level in lung among other organs. For compound heterozygotes (CH), the events with at least one deleterious allele were identified in 15 sharing/recurrent CH genes and distributed among 16 CPAM families (Table). As above, 13 of 15 CH genes were reported in adenocarcinoma in COSMIC dataset. Similarly, we identified 20 recurrent, physical protein-protein interaction pairs with digenic inheritance mutations distributed among 16 families. One protein inherited at least one rare non-synonymous variants from the father, and the other protein has another inherited rare non-synonymous mutation from the mother. Only recurrent interactive pairs were selected.

A gene with different damaging inheritance variants in different individuals (recurrently mutated gene) was identified pathogenicity. In total,

TABLE. Genetic profile of the rare damaging genetic variations in patients with congenital pulmonary airway malformation (CPAM)*

Trio	De novo	Homo	CH	Digenic	Recurrent genic copy number variant*
CPAM11		LTBP2 , <i>PGAM2</i>	<i>CCDC150</i> , <i>CUBN</i> , TTN	<i>TG</i> , <i>LRP2</i> ; <i>FASN</i> , <i>AOAH</i> ; KIAA0232 , <i>OBSL1</i>	
CPAM13	<i>MICAL2</i> , <i>SCYL1</i>	ASCC1	<i>DNAH17</i> , <i>PNPLA7</i> , TTN	<i>LASP1</i> , PRKG1 ; C5 , C7 ; <i>HIST1H2AK</i> , <i>PCF11</i> ; <i>SEMA4A</i> , <i>PLXNB1</i> ; <i>BEAN1</i> , <i>NEDD4</i> ; <i>PRKDC</i> , <i>SMG1</i>	C5
CPAM14				<i>LASP1</i> , PRKG1 ; <i>TNK1</i> , <i>SRRM2</i>	
CPAM15		<i>AR</i> , <i>BNC1</i> , <i>KIR2DS4</i> , <i>MYL10</i>	CEP128 , CEP295 , <i>CUBN</i> , <i>FOCAD</i>	<i>CFD</i> , <i>HPX</i> ; <i>MLH1</i> , <i>MSH3</i> ; <i>FASN</i> , TTN ; OBSCN , TTN ; KIAA0232 , <i>OBSL1</i>	CEP128 , FAT3 , PRKG1
CPAM16	<i>CHPF</i> , <i>CAMKK2</i>	<i>GLI1</i>	<i>PAPLN</i> , <i>SPTBN5</i> , TTN	<i>MAP2</i> , <i>KIF21B</i>	
CPAM18	<i>IMPDH1</i>	<i>PHKA1</i>		<i>FASN</i> , TTN ; <i>FASN</i> , <i>AOAH</i> ; <i>FN1</i> , <i>AOAH</i> ; OBSCN , TTN	
CPAM19	<i>CASQ2</i>	<i>ZNF467</i>	TTN	OBSCN , TTN ; <i>FASN</i> , <i>AOAH</i> ; <i>FN1</i> , <i>AOAH</i>	
CPAM2	<i>TTC27</i>	<i>LCN1</i>	<i>DNAH17</i> , <i>PNPLA7</i>		
CPAM20			<i>AHNAK2</i> , FAT3 , <i>MYBBP1A</i>	<i>MAP2</i> , <i>KIF21B</i> ; C5 , C7 ; <i>CFD</i> , <i>HPX</i> ; <i>SEMA4A</i> , <i>PLXNB1</i>	
CPAM22	<i>EPG5</i>	LTBP2 , <i>TBCC</i>	CEP128 , FAT3 , <i>SPTBN5</i> , SYNE1	<i>MLH1</i> , <i>MSH3</i>	
CPAM23	CEP295		<i>OBSCN</i> , <i>TTN</i>	<i>TLN2</i> , KIAA0232	C5
CPAM24	<i>FPGS</i>		<i>MYBBP1A</i>	<i>HIST1H2AK</i> , <i>PCF11</i>	
CPAM25	<i>CKB</i>	<i>UGT1A3</i>	C7 , OBSCN , TTN	<i>TG</i> , <i>LRP2</i> ; <i>CARD6</i> , SYNE1 ; <i>TLN2</i> , KIAA0232	
CPAM28	<i>TRIP12</i>	<i>GPR84</i> , <i>RFX6</i>	CEP295	<i>TNK1</i> , <i>SRRM2</i>	
CPAM30		<i>EDA2R</i> , <i>EGFL6</i> , <i>FXSD4</i> , <i>GANAB</i> , <i>PEPD</i>	<i>AHNAK2</i> , <i>CCDC150</i> , TTN	<i>BTRC</i> , <i>IKBKB</i> ; <i>CARD6</i> , SYNE1 ; <i>PRKDC</i> , <i>IKBKB</i>	
CPAM31			<i>PAPLN</i> , SYNE1 , TTN		
CPAM6	<i>ING1</i>	<i>HEPH</i> , <i>LHB</i> , <i>SMAD7</i>	<i>DNAH17</i> , <i>FOCAD</i>	<i>BEAN1</i> , <i>NEDD4</i>	ASCC1
CPAM9			C7 , TTN	<i>PRKDC</i> , <i>SMG1</i> ; <i>PRKDC</i> , <i>IKBKB</i>	

* Genes contained in copy number variants. **Bold** indicates that the genes are recurrently mutated in different inheritance modes.



we identified 81 genes with rare mutations including recurrently mutated gene in either CH or digenic inheritance modes, and as well as *de novo* or in homozygosis. Importantly, the alleles of recurrently mutated genes are not necessarily the same (gene mutated at different sites).

Gene-based and gene-set-based association test

To boost power for association analysis, we attempted to account for biological or functional relatedness by resorting to pathway (MsigDB) databases to group rare variants for association test. Gene-set-based (pathways) association tests revealed only one gene set reaching marginal significance in burden test ($P < 9.04391E-05$). The pathway corresponded to that of medulloblastoma tumours in mice. The top five pathways included genes with unmethylated DNA in lung cancer samples (38 genes). The case-control association test indicated the same deleterious direction between CPAM and control samples with P values of $3.57e^{-3}$, $1.96e^{-3}$, $2.71e^{-3}$ in SKAT, SKATO, and Burden tests, respectively. All CPAM patients were ‘genetically’ linked (Fig).

Searching functional overlap among genes

To understand how these mutated genes in our patients contributed to CPAM and to consider whether our findings fit into any pathological process, we performed gene/pathway-set enrichment analyses and carefully examined the genetic profile or mutational load of each patient. The gene-set enrichment test indicates several cancer-related gene-sets including Ewing’s sarcoma and prostate

cancer ($P=1.55e^{-6}$ and $P=2.28e^{-6}$, respectively). The genetic profile of each of the 18 CPAM patients is shown in the Table.

Discussion

We investigated the lesions in the genome that might be underlying CPAM. We used a straight forward design according to the presentation and incidence of the disease in the paediatric population by studying both coding sequence mutations and copy number variants. The highlights of our findings are: (1) most mutated genes are implicated in cancers of the lung and congenital soft tissue sarcomas; (2) *ASCC1* is highly expressed in lung cancer and is implicated in oesophageal adenocarcinoma and is found recurrently mutated twice, with one event being a homozygous point mutation and the other being a complete gene deletion; (3) mutations in genes encoding interacting proteins member of pathways implicated in cancer development were also recurrently detected; and (4) mutation recurrence was observed for both point coding DNA sequence mutations and copy number variants.

Despite heterogeneity, our findings provide a pathway to look for a therapeutic target. Although our data need to be replicated, and functional assays are needed, it is a lead that hopefully the rest of the scientific community will follow.

An inherent limitation to this project (and to any other project involving a genetic study of a rare genetic heterogenic and oligo/polygenic disorder) is the small sample size and/or the lack of large pedigrees where the disease segregated. When different genes are thought to underlie the same disorder, a large sample size is needed so that genes recurrently mutated can be identified. Intuitively, the different genes underlying the disorder should be connected through a pathway, yet, not all pathways or connectivity are known. Replication has not been done as the number of samples is insufficient.

Acknowledgements

This study was supported by the Health and Medical Research Fund, Food and Health Bureau, Hong Kong SAR Government (#01121576). We thank the patients who participated in the study.

References

1. Wilson RD, Hedrick HL, Liechty KW, et al. Cystic adenomatoid malformation of the lung: review of genetics, prenatal diagnosis, and in utero treatment. *Am J Med Genet A* 2006;140:151-5.
2. Kayton ML, He M, Zakowski MF, et al. Primary lung adenocarcinomas in children and adolescents treated for pediatric malignancies. *J Thorac Oncol* 2010;5:1764-71.
3. DeBoer EM, Keene S, Winkler AM, Shehata BM. Identical twins with lethal congenital pulmonary airway malformation type 0 (acinar dysplasia): further evidence of familial tendency. *Fetal Pediatr Pathol* 2012;31:217-24.

Exome sequencing to reveal presymptomatic genetic markers for primary open angle glaucoma

LJ Chen *, CP Pang, CCY Tham, CKS Leung

KEY MESSAGES

1. *MEGF11* was identified as a new putative disease-causing gene for primary open angle glaucoma (POAG) in a Chinese population.
2. Mutations in *MEGF11* contributed to about 1.1% of Chinese patients with POAG.
3. The association of variant rs4236601 in the *CAVI/CAV2* gene locus with POAG in Chinese patients is confirmed.
4. A common variant in this locus, rs3801994, is suggested as a new genetic biomarker for POAG in Chinese patients.

5. Both *MEGF11* and *CAVI/CAV2* gene loci are excellent genetic biomarkers that can be incorporated into future genetic diagnostic platforms for POAG.

Hong Kong Med J 2019;25(Suppl 5):S39-43

HMRP project number: 01122236

LJ Chen, CP Pang, CCY Tham, CKS Leung

Department of Ophthalmology and Visual Sciences, The Chinese University of Hong Kong

* Principal applicant and corresponding author: lijia_chen@cuhk.edu.hk

Introduction

Glaucoma is the leading cause of irreversible blindness worldwide. The majority of glaucoma cases are primary open-angle glaucoma (POAG), which is caused by interactions of multiple environmental and genetic risk factors. In the complex form of POAG, many genes can be involved, each having a small-to-moderate effect. By contrast, in the Mendelian form of POAG, mutations are usually in a single gene.

Different genetic strategies have been applied to identify POAG genes. With the advent of the next-generation sequencing, most or all types of genomic variation in all exons (ie, the exome) can be detected. The exome constitutes approximately 1% of the whole genome, and approximately 85% of causal mutations for human diseases are located within its coding region and splice sites.¹

In a previous study, *TCF4* rs613872 was found to be strongly associated with Fuchs corneal dystrophy in Caucasians but not in Chinese, whereas single-nucleotide polymorphisms (SNPs) in *PMP22* were not associated with Fuchs corneal dystrophy in Caucasians or Chinese populations.² Therefore, we did not involve these two genes in the present study. In this study, we used exome sequencing, Sanger sequencing, and SNP genotyping to identify new causative and susceptible gene variants for POAG.

Methods

Study subjects

Five Chinese pedigrees with POAG were recruited for exome sequencing, as were >500 unrelated Chinese POAG patients with variable age of onset, highest intraocular pressure before treatment, and disease

severity, as well as >500 unrelated control subjects who had normal visual acuity, no major ocular disorders except for mild senile cataract or refractive errors if any, intraocular pressure <21 mmHg. All patients, family members, and control subjects underwent detailed ophthalmic examination.

Exome sequencing and mutation analysis

For exome sequencing, all available affected and unaffected family members in the POAG pedigrees were included. Total DNA was extracted from peripheral blood using standard protocols for exome sequencing. A pipeline data analysis was used to determine the disease-causing mutations. Segregation analysis was performed after filtering of variants. The variants that are completely segregated with the disease (ie, those occur in patients only but not in controls) were considered as candidate disease-causing mutations. In order to determine the mutation frequency of the newly identified gene (*MEGF11*) in POAG in the Chinese population, all exons of the gene were sequenced in the >500 unrelated patients with POAG using Sanger sequencing. Subsequently, the mutations detected were excluded in the >500 controls to determine the causality of the mutations.

Evaluation of the *CAV1/2* gene associated with POAG

By using the sample set and the genetic information, we also evaluated the role of *CAV1/2* gene locus in POAG in three Chinese cohorts from Hong Kong, Shantou (southern Chinese) and Beijing (northern Chinese). We investigated seven SNPs, including rs4236601 that was reported in the previous GWAS³

and six haplotype-tagging SNPs covering the *CAV1/CAV2* locus based on the Chinese Han Beijing population in HapMap project (namely rs6466579, rs7801950, rs3779512, rs3807989, rs3801994, and rs1049337).

Data processing and analysis

Bioinformatics analysis was performed for all candidate mutations. Online computer programmes (eg, PolyPhen2, SIFT, and the ASSA) were used to predict the potentially functional impacts of each missense or nonsense variant to the protein or to alternative splicing. Genetic association and genotype-phenotype correlation analyses were performed using chi-square test and logistic regression.

Results

In the five Chinese POAG pedigrees, the exome sequencing data included all annotated variants such as single nucleotide variants, small deletions and insertions (indels), and splice site variants in the exon-intron junctions. After the pipeline filtering procedure and segregation analysis, we found no single variant that was completely cosegregated with POAG in any of the three POAG pedigrees. Therefore, exome sequencing alone did not identify disease-causing gene for POAG.

We then reviewed the data in one of the pedigrees, which is the *GLC1N*-linked POAG family.⁴ We narrowed the targeted variants to the *GLC1N* region (15q 22-24). In this family, we identified

one deletion mutation c.1090delT in the *MEGF11* gene to be segregated with POAG in the pedigree except one married-in subject (II:15) [Fig 1]. This mutation is predicted to cause a large C-terminal protein truncation of *MEGF11* (p.Cys364ValfsX12). It is therefore likely glaucoma related. Sequencing analysis of this deletion in the rest of the family members who had no identifiable sign of glaucoma at the time of recruitment, revealed its presence in another four kindred members (III:4, III:6, III:16, and III:17), of whom III:16 was a homozygote (Fig 2). With the unexpected founding of the mutation in the married-in husband II:15, we recruited the kindred members of II:15 (ie, II:15M and II:15S) and found the deletion in subject II:15S and not II:15M (Fig 1). So both II:15 and II:15S, aged 46 and 47 years, respectively, at the time of recruitment, were heterozygous for *MEGF11* c.1090delT but they did not have glaucoma. These two families are unrelated. Thus, the *MEGF11* c.1090delT mutation seems necessary, but not sufficient, for the pathogenesis of glaucoma in the *GLC1N*-linked family.

We then screened the *MEGF11* coding sequence in another 453 unrelated POAG patients and identified the c.1090delT deletion in a male Chinese POAG patient from the Beijing cohort. This deletion was absent in 529 Chinese. We also identified three splice site mutations (IVS17+2insT, IVS17-4C>G and c.2472A>C) in patients but not in controls (Table).

Association of *CAV1/CAV2* with POAG

SNP rs4236601, which was identified in the

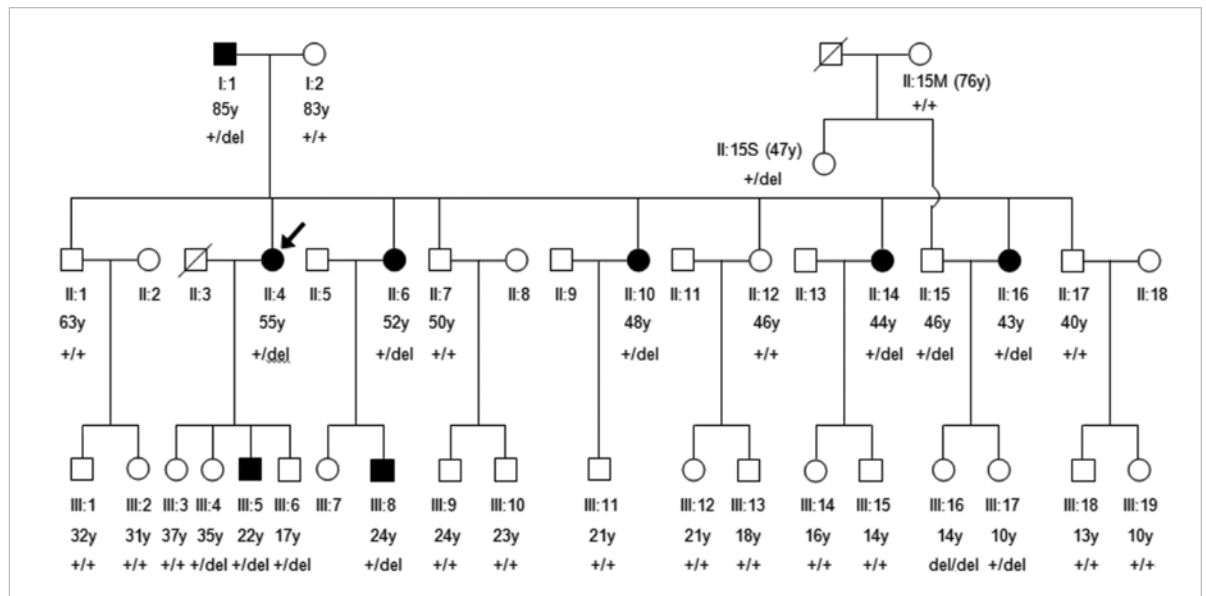


FIG 1. Segregation of *MEGF11* c.1090delT in the *GLC1N*-lined pedigree with primary open angle glaucoma. The genotype of the c.1090delT mutation is shown, where +/+ represents the wild-type, +/- represents heterozygote, and del/del represents homozygote

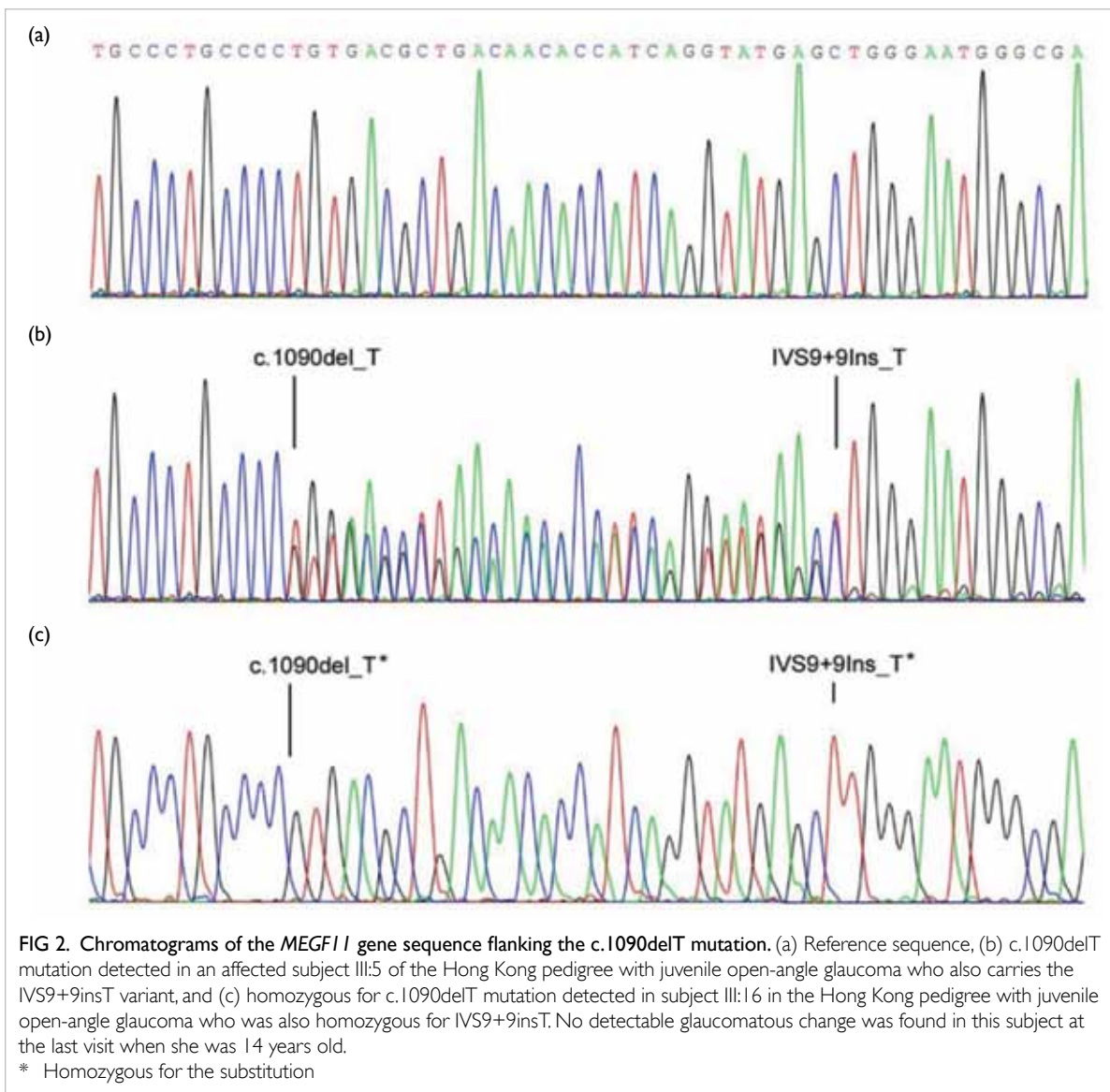


FIG 2. Chromatograms of the *MEGF11* gene sequence flanking the c.1090delT mutation. (a) Reference sequence, (b) c.1090delT mutation detected in an affected subject III:5 of the Hong Kong pedigree with juvenile open-angle glaucoma who also carries the IVS9+9insT variant, and (c) homozygous for c.1090delT mutation detected in subject III:16 in the Hong Kong pedigree with juvenile open-angle glaucoma who was also homozygous for IVS9+9insT. No detectable glaucomatous change was found in this subject at the last visit when she was 14 years old.
* Homozygous for the substitution

GWAS,³ conferred an increased risk of POAG (A allele, $P=0.0072$, odds ratio [OR]=4.72), with a population attributable risk of 1.47%. A common SNP, rs3801994, showed a borderline association with POAG (A allele, $P=0.036$, OR=1.31). This SNP conferred a population attributable risk of 4.33%. Based on the findings in the Hong Kong cohort, we genotyped the SNPs rs4236601 and rs3801994 in the cohorts from Shantou, Beijing, and Osaka. SNP rs4236601 was associated with POAG in the Shantou cohort ($P=0.0079$, OR=4.23). Also, rs4236601 showed a significant association with POAG in the Beijing cohort after adjusting for age and gender ($P=0.030$, OR=3.92). In contrast, rs3801994 was not significantly associated with POAG in the Shantou or Beijing cohort, but their ORs were toward the same direction with that in the Hong Kong cohort. By pooling the data of rs4236601 and rs3801994 from the 3 Chinese cohorts, the SNP rs4236601 was

strongly associated with POAG prior to ($P=1.1 \times 10^{-4}$, OR=3.80), with no inter-cohort heterogeneity ($I^2=0$). SNP rs3801994 showed a borderline association with POAG ($P=0.022$, OR=1.23, $I^2=0$).⁵

Discussion

Although exome sequencing alone did not lead to the identification of a disease-causing gene for POAG in the five POAG pedigrees, the combination of exome sequencing data and our previous linkage study in a Hong Kong Chinese POAG pedigree identified a novel deletion mutation c.1090delT in the *MEGF11* gene to be implicated in POAG. The mutation was deemed necessary for glaucoma pathogenesis in the POAG pedigree. This mutation was also detected in a Chinese POAG patient from the Beijing cohorts but was absent in 529 unrelated Chinese. Therefore, this *MEGF11* deletion is likely to be pathogenic

TABLE. Distribution of rare variants of *MEGF11* in patients with primary open angle glaucoma (POAG) and controls*

Variation category	Hong Kong cohort		Beijing cohort		Shantou cohort		Pooled Chinese subjects	
	POAG (n=181)	Control (n=182)	POAG (n=177)	Control (n=200)	POAG (n=95)	Control (n=147)	POAG (n=453)	Control (n=382)*
Coding variants								
Any coding variants (variants present in both cases and controls inclusive)	14 (7.7)	13 (7.1)	9 (5.1)	11 (5.5)	4 (4.2)	ND	27 (6.0)	24 (6.3)
Missense variants	10 (5.5)	10 (5.5)	6 (3.4)	5 (2.5)	2 (2.1)	ND	18 (4.0)	15 (3.9)
Variants predicted damaging (PolyPhen)	2 (1.1)	5 (2.8)	1 (0.6)	4 (2.0)	1 (1.1)	ND	4 (0.9)	9 (2.4)
Variants predicted benign (PolyPhen)	8 (4.4)	5 (2.8)	5 (2.8)	1 (0.5)	1 (1.1)	ND	14 (3.1)	6 (1.6)
Variants in EGF-like domains	2 (1.1)	1 (0.6)	2 (1.1)	1 (0.5)	1 (1.1)	ND	5 (1.1)	2 (0.5)
Variants in EGF-like domains and predicted damaging	0	1 (0.6)	0	1 (0.5)	1 (1.1)	ND	1 (0.2)	2 (0.5)
Variants result in premature truncation	1 (0.6)	0	1 (0.6)	0	0	ND	2 (0.4)	0/529
Coding variants exclusively present in cases/controls	9 (5.0)	9 (5.0)	7 (4.0)	6 (3.0)	2 (2.1)	ND	18 (4.0)	15 (3.9)
Missense variants exclusively present in cases/controls	7 (3.9)	6 (3.3)	4 (2.3)	2 (1.0)	2 (2.1)	ND	13 (2.9)	8 (2.1)
Damaging variants exclusively present in cases/controls	3 (1.7)	5 (2.8)	1 (0.6)	2 (1.0)	1 (1.1)	ND	5 (1.1)	7 (1.8)
Intronic variants								
Any intronic variants	8 (4.4)	7 (3.9)	10 (5.6)	14 (7.0)	2 (2.1)	ND	20 (4.4)	21 (5.5)
Variants at invariant AG/GT splice acceptor/donor site	0	0	0	0	1 (1.0)	ND	1 (0.2)	0

* No significant difference detected for each comparison of the proportion

† Included only controls from the Hong Kong and Beijing cohorts. For the truncation mutation, controls were pooled from the three cohorts (n=529)

for POAG. However, four mutation carriers in the pedigree (III:4, III:6, III:16, and III:17) were found without glaucomatous features at the time of study enrolment. Moreover, subject III:16 was homozygous for the deletion while her father (II:15) and aunt (II:15S), from a different pedigree, were unaffected mutation carriers. The *MEGF11* c.1090delT is thus likely to be the causal mutation for POAG in this *GLC1N*-linked family with incomplete penetrance.

Additionally, we identified three splice junction mutations, which are likely to result in leaky splice sites, in three patients. These four mutations are likely to result in *MEGF11* proteins lacking one of the 15th, 16th, and 17th EGF-like domains, suggesting that absence of either one of these domains could be pathogenic for glaucoma. If these four putative mutations, namely c.1090delT, IVS17+2insT, IVS17-4C>G, and c.2472A>C, are in fact pathogenic, the *MEGF11* mutations may contribute to approximately 1.1% (5/453) of index POAG patients in Chinese.

We also confirmed the association between SNP rs4236601 at the *CAVI/CAV2* locus and POAG in Chinese. The minor allele A increased the risk of POAG by over fourfold in southern Chinese and nearly threefold in northern Chinese. Moreover, we identified a common SNP rs3801994 for POAG

in Chinese, with an OR of 1.23. Thus, our data highlighted an important role of the *CAVI/CAV2* gene in the genetic susceptibility of POAG.

The mutation frequency of *MEGF11* (1.1%) and the population attributable risk of *CAVI/CAV2* (4.33%) are low, therefore to design a diagnostic gene chip based on the current findings provides limited practical value. However, they are excellent candidate genes that should be incorporated into future gene chips for the genetic diagnosis of POAG, especially for Hong Kong Chinese population.

Conclusions

MEGF11 is likely a causative gene of POAG, contributing to 1.1% of POAG patients in the Chinese population. rs4236601 is associated with POAG in the southern and northern Chinese. A common SNP at the *CAVI/CAV2* locus, rs3801994, is suggested as a new genetic biomarker for POAG in Chinese. Further genetic studies are needed to identify more genetic biomarkers for POAG.

Acknowledgements

This study was supported by the Health and Medical Research Fund, Food and Health Bureau, Hong Kong

SAR Government (#01122236). We also thank all the participants in this study.

Results from this study have been published in:

- (1) Rong SS, Chen LJ, Leung CK, et al. Ethnic specific association of the CAV1/CAV2 locus with primary open-angle glaucoma. *Sci Rep* 2016;6:27837, and
- (2) Lau LC, Ma L, Young AL, et al. Association of common variants in TCF4 and PTPRG with Fuchs' corneal dystrophy: a systematic review and meta-analysis. *PLoS One* 2014;9:e109142.

References

1. Choi M, Scholl UI, Ji W, et al. Genetic diagnosis by whole exome capture and massively parallel DNA sequencing. *Proc Natl Acad Sci U S A* 2009;106:19096-101.
2. Lau LC, Ma L, Young AL, et al. Association of common variants in TCF4 and PTPRG with Fuchs' corneal dystrophy: a systematic review and meta-analysis. *PLoS One* 2014;9:e109142.
3. Thorleifsson G, Walters GB, Hewitt AW, et al. Common variants near CAV1 and CAV2 are associated with primary open-angle glaucoma. *Nat Genet* 2010;42:906-9.
4. Wang DY, Fan BJ, Chua JK, et al. A genome-wide scan maps a novel juvenile-onset primary open-angle glaucoma locus to 15q. *Invest Ophthalmol Vis Sci* 2006;47:5315-21.
5. Rong SS, Chen LJ, Leung CK, et al. Ethnic specific association of the CAV1/CAV2 locus with primary open-angle glaucoma. *Sci Rep* 2016;6:27837.

Modulation of the PTEN/mTOR pathway to enhance survival of cone photoreceptors in retinal degeneration disorders

B Lin*

KEY MESSAGES

1. Phosphatase and tensin homologue (PTEN) overexpression down-regulated mTOR and S6K1 activity and induced 661W cone cell apoptosis.
2. S6K1 knockdown prevented 661W cone cell survival to a similar degree as PTEN.
3. S6K1 expression improved 661W cone survival in the presence of PTEN.
4. PTEN deletion activated S6K1 and improved the survival and function of cones and visual performance in the rd10 mouse model of retinitis pigmentosa.
5. S6K1 treatment rescued cones from degeneration in the rd10 retina.

Hong Kong Med J 2019;25(Suppl 5):S44-7

HMRF project number: 01120856

B Lin

School of Optometry, The Hong Kong Polytechnic University

* Principal applicant and corresponding author: b.lin@polyu.edu.hk

Introduction

Retinitis pigmentosa refers to a type of inherited retinal photoreceptor degeneration. Mutations in rod-specific genes cause photoreceptor death, and cones die subsequent to the rod cell loss in this disease.¹ The molecular mechanisms that lead to the secondary cone death are not fully understood. Down-regulation of the insulin/mTOR metabolic pathway has been reported to be a major cause of cone death in several mouse models of retinitis pigmentosa.² Down-regulation of the PI3K/mTOR pathway can be modulated at several levels. For instance, phosphatase and tensin homologue (PTEN) opposes PI3K function, leading to inactivation of the PI3K/mTOR pathway. However, it remains unclear whether inactivation of the PI3K/mTOR pathway is directly modulated by PTEN in retinitis pigmentosa. To determine whether PTEN is involved in down-regulating the PI3K/mTOR pathway, we used the Cre-loxP system to generate a cone-specific deletion of PTEN to assess the effect of PTEN deletion on the PI3K/mTOR pathway and on the structural integrity and function of cones in the rd10 mouse model of retinitis pigmentosa.³

Methods

Wild-type (C57BL/6) mice, rd10 mice, and PTEN^{loxP/loxP} mice were obtained from Jackson Laboratory (Bar Harbor [ME], US). To investigate whether PTEN deletion slowed down cone degeneration in rd10 retinas, rd10 mice were backcrossed with PTEN^{loxP/loxP} mice, and the littermates from rd10/PTEN^{loxP/loxP} mice and rd10/PTEN^{+/-loxP} mice were used for experiments.

The plasmid CAG-Cre was purchased from Addgene (#13775). The plasmid human red opsin promoter-Cre was constructed by replacing CAG with a human red opsin promoter. To create a conditional PTEN deletion in cone photoreceptors, we injected an adeno-associated virus vector expressing Cre driven by a human red opsin

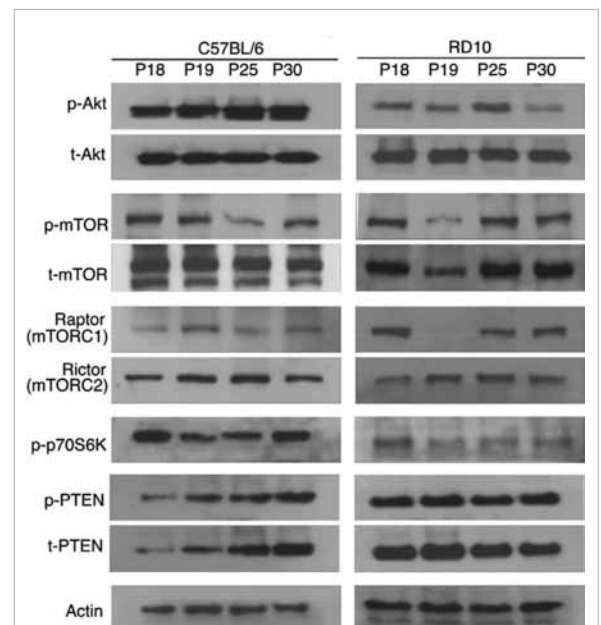


FIG 1. PI3K/mTOR pathway dysregulated in rd10 retinas.

Western blots of whole retinal phosphorylated Akt (p-Akt) and total Akt (t-Akt), p-mTOR and t-mTOR, Raptor (mTORC1), Rictor (mTORC2), p-p70S6K, p-PTEN, and t-PTEN from rd10 mice and C57BL/6 mice. β -actin levels were used as a loading control. The PI3K/mTOR pathway was downregulated, and PTEN was upregulated in rd10 retinas.

promoter. DNA (0.5 μ l of 5 μ g/ μ l) was injected into the subretinal space of right eyes of newborn mouse pups. After DNA injection, 80V pulses were applied using a square pulse electroporator ECM830.

We then assessed Cre expression and cellular localisation in retinas by immunofluorescence staining using an anti-Cre antibody. To ensure that cones were selectively targeted, we stained Cre-treated PTEN^{loxP/loxP}/rd10 retinas using both anti-Cre and anti-red/green opsin antibodies. Primary antibodies used were rabbit anti-red/green opsin, rabbit anti-blue opsin, and rabbit anti-Cre recombinase. A secondary antibody conjugated to either Alexa 488 or Alexa 594 was applied for 2 hours at room temperature. Confocal micrographs of fluorescent specimens were captured using a Zeiss LSM 700 Meta Axioplan 2 laser scanning confocal

microscope (Carl Zeiss, Oberkochen, Germany) equipped with argon and helium-neon laser.

We assessed the effect of PTEN deletion on photoreceptor function using scotopic and photopic electroretinography (with an Espion ERG Diagnostics machine). Scotopic, rod-mediated responses were obtained from dark-adapted animals. Photopic, cone-mediated responses were performed following 10-minute light adaptation.

Vertical sine wave gratings were projected on computer monitors. Images of head movements were monitored using an infrared-sensitive camera.

661W cells were transfected with a mixture composed of lipofectamine 2000 (Invitrogen) and pCMV/Flag/WT-PTEN, with over-expression of pCMV/Flag/dPDZ-PTEN as the negative control. p70S6K1 overexpression was realised by transfecting

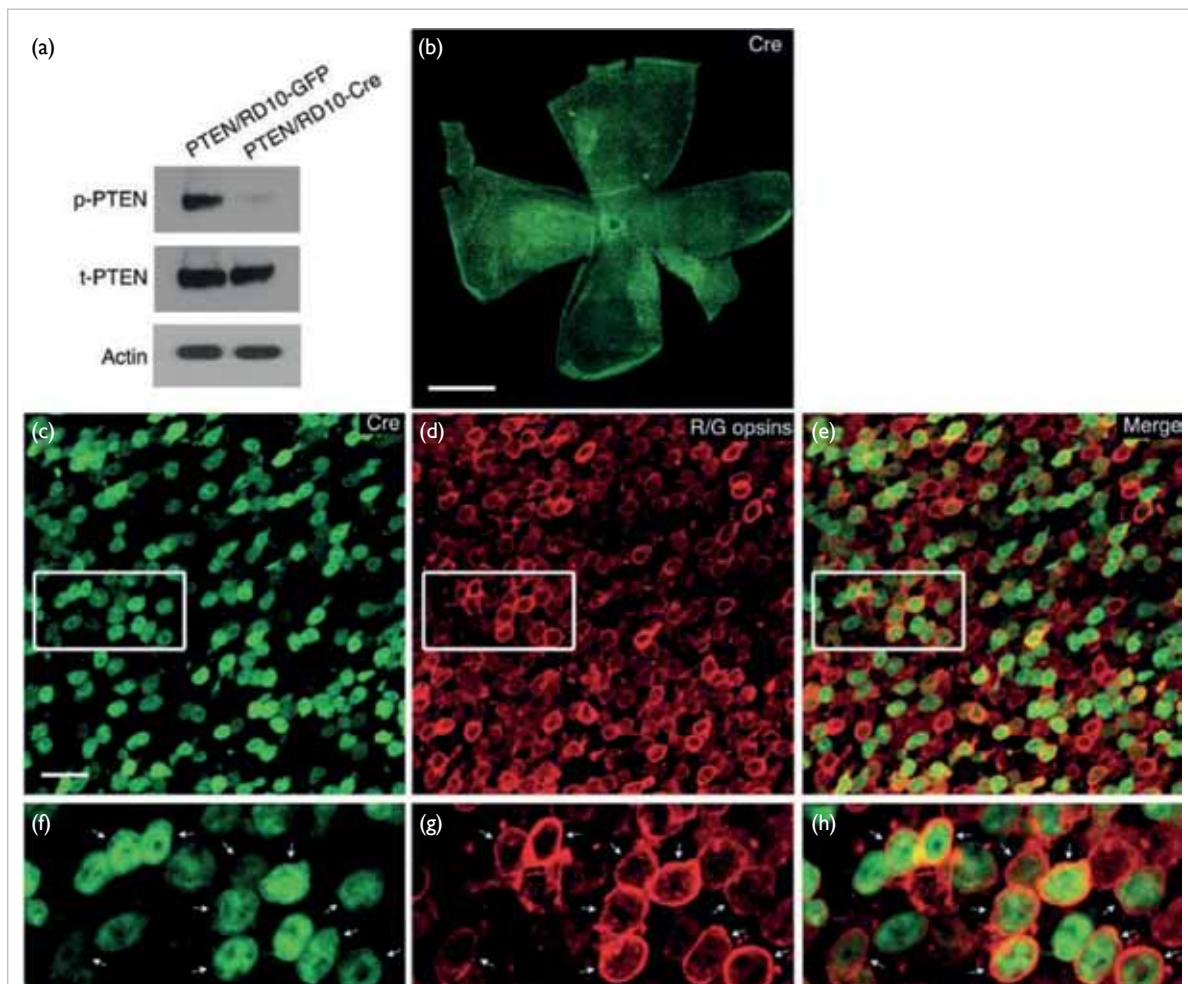


FIG 2. Conditional deletion of PTEN in cone photoreceptors of rd10 mice. (a) Western blots of PTEN protein levels in Cre-treated PTEN^{loxP/loxP}/rd10 mice and GFP-treated PTEN^{loxP/loxP}/rd10 mouse retinas. β -actin levels were used as a loading control. (b) Flat mounted preparation of rd10/PTEN^{loxP/loxP} mice treated with adeno-associated virus vector expressing Cre and harvested at P25. Representative retinal flat mount showed extensive Cre expression stained by an anti-Cre antibody (green) throughout the whole retina. Adeno-associated virus-human red opsin promoter-Cre-treated PTEN^{loxP/loxP}/rd10 retinas were co-labelled with antibodies against (c) Cre (green) and (d) red/green opsins (red). (e) Most cre-positive cells were also positive for red/green opsins. (f to h) Highly magnified images of the boxed regions above. Red/green cones colocalised with Cre (arrows).

pRK7-HA-S6K1-WT, and pRK7-HA-S6K1-KR was used as the negative control.

The total and phosphorylated forms of PTEN, Akt, Raptor, Rictor, mTOR, and p70S6K proteins were measured using western blot analysis.

Results

Phosphorylated PTEN was upregulated, whereas phosphorylated Akt, phosphorylated mTOR, mTORC1 and p70S6K were downregulated in the rd10 retina relative to control retinas (Fig 1). These suggested the possible correlation between down-regulation of PI3K/Akt survival pathway and up-regulation of PTEN in rd10 retinas.

PTEN overexpression increased the proportion of TUNEL positive 661W cells (data not shown). p70S6K1 knockdown induced 661W cone cell apoptosis. S6K1 increased cell survival in PTEN-overexpressed 661W cone cells. These data

confirmed that PTEN functions through p70S6K1 to regulate cone cell apoptosis.

Most Cre-positive cells were co-labelled with red/green opsins, indicating specific Cre transduction in cones (Fig 2).

Scotopic b-wave amplitudes at two different light intensities were significantly higher in Cre-treated PTEN^{loxP/loxP}/rd10 mice than in GFP-treated PTEN^{loxP/loxP}/rd10 mice (Fig 3). Photopic electroretinographic a- and b-wave amplitudes in Cre-treated PTEN^{loxP/loxP}/rd10 mice were similarly larger compared to GFP-treated PTEN^{loxP/loxP}/rd10 controls (Fig 3). Additionally, we measured the optomotor response of mice to moving gratings. Photopic visual acuity was approximately 2.5-fold higher in P35 Cre-treated PTEN^{loxP/loxP}/rd10 mice than that in age-matched GFP-treated PTEN^{loxP/loxP}/rd10 (Fig 3g). Taken together, PTEN deletion improved retinal function and visual performance in rd10 mice.

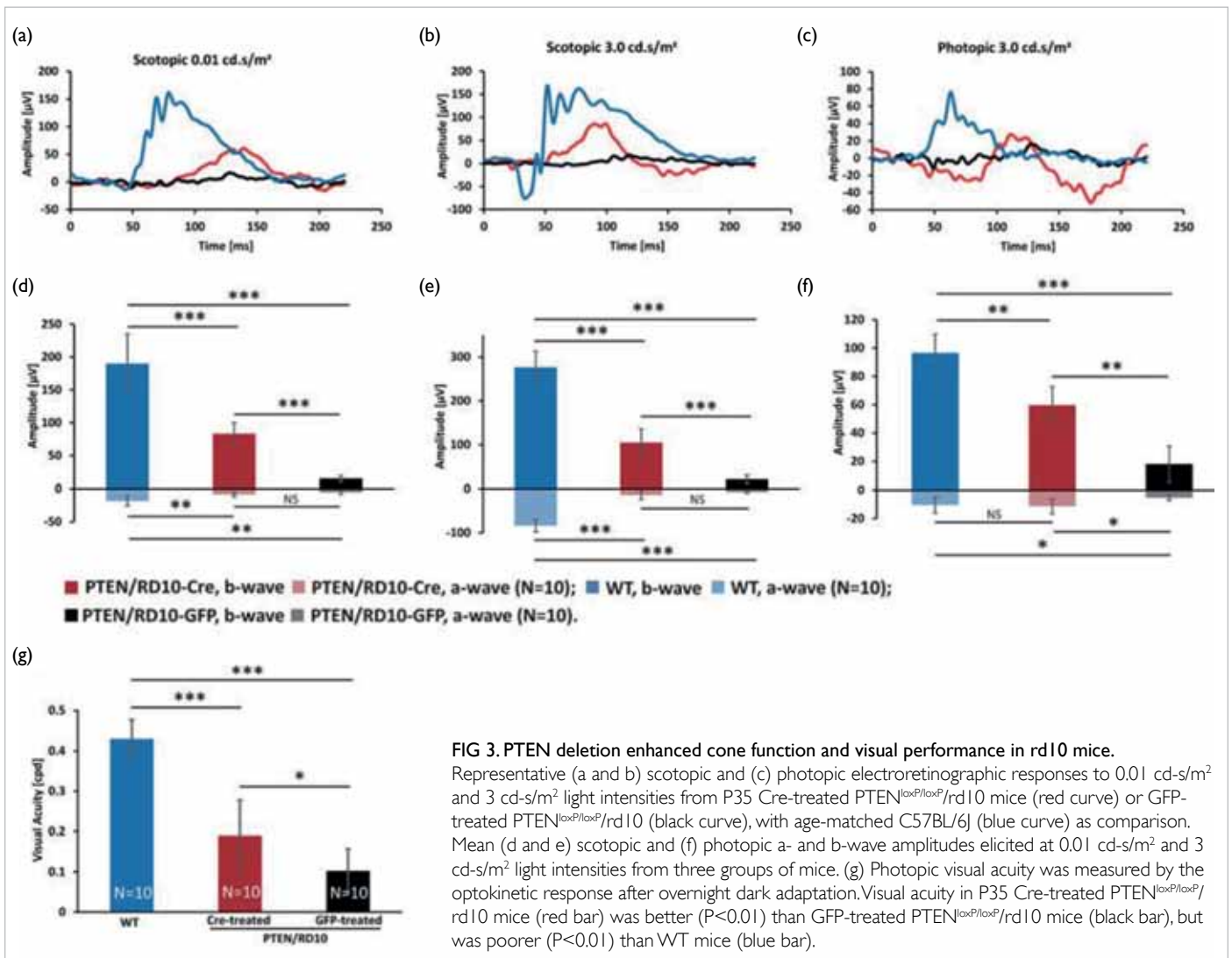


FIG 3. PTEN deletion enhanced cone function and visual performance in rd10 mice. Representative (a and b) scotopic and (c) photopic electroretinographic responses to 0.01 cd.s/m² and 3 cd.s/m² light intensities from P35 Cre-treated PTEN^{loxP/loxP}/rd10 mice (red curve) or GFP-treated PTEN^{loxP/loxP}/rd10 (black curve), with age-matched C57BL/6j (blue curve) as comparison. Mean (d and e) scotopic and (f) photopic a- and b-wave amplitudes elicited at 0.01 cd.s/m² and 3 cd.s/m² light intensities from three groups of mice. (g) Photopic visual acuity was measured by the optokinetic response after overnight dark adaptation. Visual acuity in P35 Cre-treated PTEN^{loxP/loxP}/rd10 mice (red bar) was better (P<0.01) than GFP-treated PTEN^{loxP/loxP}/rd10 mice (black bar), but was poorer (P<0.01) than WT mice (blue bar).

Discussion

PTEN activity played a major role in down-regulating the PI3K/mTOR survival pathway and contributed to photoreceptor apoptosis in the rd10 mouse model of retinitis pigmentosa. Conversely, PTEN deletion in cones activated the PI3K/mTOR pathway and subsequently facilitated cone photoreceptor survival. PTEN overexpression induced 661W cone cell apoptosis by direct inhibition of the PI3K/mTOR survival pathway. Furthermore, S6K1 was identified as one of the downstream effectors of PTEN neurotoxicity. The effect of PTEN demonstrated *in vitro* was further confirmed *in vivo* by conditional deletion of PTEN in cone photoreceptors of rd10 mouse retinas. PTEN deficiency activated the PI3K/mTOR pathway and its downstream target S6K1, enhanced cone survival and function, and improved visual performance in rd10 mice, confirming that

PTEN activation contributed to the induction of cone death in rd10 retinas.

Acknowledgement

This study was supported by the Health and Medical Research Fund, Food and Health Bureau, Hong Kong SAR Government (#01120856).

References

1. Hartong DT, Berson EL, Dryja TP. Retinitis pigmentosa. *Lancet* 2006;368:1795-809.
2. Punzo C, Kornacker K, Cepko CL. Stimulation of the insulin/mTOR pathway delays cone death in a mouse model of retinitis pigmentosa. *Nat Neurosci* 2009;12:44-52.
3. Bowes C, Li T, Danciger M, Baxter LC, Applebury ML, Farber DB. Retinal degeneration in the rd mouse is caused by a defect in the beta subunit of rod cGMP-phosphodiesterase. *Nature* 1990;347: 677-80.

AUTHOR INDEX

Abrigo J	6	Li R	6
Au Yeung KC	30	Li SH	6
Chan AKY	17	Liebeskind DS	18
Chan E	22	Lin B	44
Chan HC	12	Lin WH	9
Chan LW	30	Lo AWI	17
Chen LJ	39	Lo TK	30
Chen XY	9	Ma ESK	3
Cheung ANY	33	Mok V	22
Choy RKW	30	Ng PW	6
Chu W	6	Ngan HYS	33
Collins RA	3	Pang CP	39
Dai EYL	18	Poon WS	17
Fan SY	18	Sahota DS	30
Fong WC	6	Siu DYW	9, 18, 22
Ip HL	18	Soo YO	6, 9
Jiang XH	12	Tam PK	36
Ke Y	26	Tham CCY	39
Kwong DWJ	26	Tian G	9
Lam PK	17	To WWK	30
Lau AYL	18, 22	Tsang LL	12
Lau KK	22	Wang YX	17
Lau WL	30	Wong GKC	17
Lee R	22	Wong KK	6
Leung CKS	39	Wong LKS	6, 9, 18
Leung KT	6	Wong OGW	33
Leung KY	30	Wong RMS	26
Leung TWH	6, 9, 18	Xiong L	9
Leung TY	30	Yang FY	12
Leung WC	30	Yung KKL	26
Li HW	26	Zhang XH	12

Disclaimer

The reports contained in this publication are for reference only and should not be regarded as a substitute for professional advice. The Government shall not be liable for any loss or damage, howsoever caused, arising from any information contained in these reports. The Government shall not be liable for any inaccuracies, incompleteness, omissions, mistakes or errors in these reports, or for any loss or damage arising from information presented herein. The opinions, findings, conclusions and recommendations expressed in this publication are those of the authors of the reports, and do not necessarily reflect the views of the Government. Nothing herein shall affect the copyright and other intellectual property rights in the information and material contained in these reports. All intellectual property rights and any other rights, if any, in relation to the contents of these reports are hereby reserved. The material herein may be reproduced for personal use but may not be reproduced or distributed for commercial purposes or any other exploitation without the prior written consent of the Government. Nothing contained in these reports shall constitute any of the authors of these reports an employer, employee, servant, agent or partner of the Government.

Published by the Hong Kong Academy of Medicine Press for the Government of the Hong Kong Special Administrative Region. The opinions expressed in the *Hong Kong Medical Journal* and its supplements are those of the authors and do not reflect the official policies of the Hong Kong Academy of Medicine, the Hong Kong Medical Association, the institutions to which the authors are affiliated, or those of the publisher.